

# Exploring the Impact of Nuclear Parton Distribution Functions on Open Heavy Flavor Azimuthal Angular Correlations in Pb-Pb Collisions at $\sqrt{s_{NN}} = 5.5$ TeV

Swapnesh Khade,<sup>1,\*</sup> Ravindra Singh,<sup>2,†</sup> Yoshini Bailung,<sup>1,‡</sup> and Ankhi Roy<sup>1,§</sup>

<sup>1</sup>*Department of Physics, Indian Institute of Technology Indore, Simrol, Indore 453552, India*

<sup>2</sup>*GSI Helmholtzzentrum für Schwerionenforschung, Darmstadt, Germany*

(Dated: August 22, 2024)

In this paper, we explore the impact of nuclear parton distribution functions (nPDFs) on the azimuthal angular correlation of open heavy flavor hadrons in Pb-Pb collisions at  $\sqrt{s_{NN}} = 5.5$  TeV, utilizing PYTHIA8 + Angantyr model and various PDFs. The method involves a transverse momentum ( $p_T$ ) differential assessment of azimuthal angular correlations between prompt  $D^0 - \bar{D}^0$ ,  $B - \bar{B}$ , and non-prompt D-mesons. The results show that nPDFs significantly modify the near-side and away-side peaks of the azimuthal angular correlation distribution. A differential  $p_T$  analysis allowed us to find the interplay between various production mechanisms and the significant impact of nPDFs on the dynamics of heavy flavor hadron production. Apart from the contributions originating from leading order (LO) production processes like pair creation in the away side correlation distribution, the identification of a double peak structure in the near side of azimuthal angular correlation indicates contributions from next-to-leading order (NLO) processes. The paper also emphasizes the relevance of nPDF in the context of heavy quark thermalization in heavy-ion collision analyses. The findings indicate that nPDFs alter charm quark thermalization at low  $p_T$ , with negligible effects on beauty quark thermalization. This comprehensive analysis of azimuthal correlations and nPDF effects enhances our understanding of the initial state conditions and the dynamics of heavy flavor production in heavy-ion collisions.

## I. INTRODUCTION

Experiments at the Large Hadron Collider at CERN, Geneva and the Relativistic Heavy Ion Collider (RHIC) at BNL, USA, explore the properties of quark-gluon plasma (QGP), an exotic state of matter, by colliding ultra-relativistic heavy-ions [1–4]. The QGP was discovered at the SPS, in Pb-Pb collisions at the center of mass energy  $\sqrt{s_{NN}} = 17.3$  GeV [5, 6], inspiring future experiments such as ALICE and STAR to perform precise measurements and understand its properties.

An evolution of heavy-ion collision comprises an initial or pre-equilibrium state, a deconfined state of partons, followed by hadronization, and ultimately, freeze-out of the final state hadrons [3]. To systematically study all the stages of a heavy-ion collision, it is necessary to use a probe that is produced at the onset of the collision and traverses through the various stages. Heavy quarks (charm and beauty), due to their large masses, are produced at the early stages of heavy-ion collision via initial hard scatterings. They experience a complete history of the heavy-ion collision and serve as excellent probes to study its various stages. While interacting with the pre-equilibrium state and the QGP medium, heavy quarks lose energy via collisional and radiative processes, which are followed by fragmentation [7–10] and hadronization

processes [11–16]. In hadronic collisions, the production of open heavy flavor hadrons [17] can be explained using the factorization theorem. For open charm hadrons, the total production cross-section is given by,

$$d\sigma_{AB \rightarrow C}^{\text{hard}} = \sum_{a,b,X} f_{a/A}(x_a, Q^2) \otimes f_{b/B}(x_b, Q^2) \otimes d\sigma_{ab \rightarrow cX}^{\text{hard}}(x_a, x_b, Q^2) \otimes D_{c \rightarrow C}(z, Q^2) \quad (1)$$

where,  $f_{a/A}(x_a, Q^2)$  and  $f_{b/B}(x_b, Q^2)$  are the parton distribution functions (PDFs) which give the probability of finding parton  $a(b)$  inside the hadron  $A(B)$  for a given  $x$ , where  $x$  is the fraction of longitudinal proton momentum taken by a parton, and  $Q^2$  is the factorization scale.  $d\sigma_{ab \rightarrow cX}^{\text{hard}}(x_a, x_b, Q^2)$  is the partonic hard scattering cross-section, and  $D_{c \rightarrow C}(z, Q^2)$  is the fragmentation function of the produced hadron. For beauty quarks, the production of B-mesons will have effects due to its higher mass than charm, which alters production cross-section and its fragmentation function [18–20]. A partonic hard scattering cross-section is calculated by perturbative quantum chromodynamic (pQCD) calculations while the fragmentation function and PDFs invoke non-perturbative treatments. The production of heavy quarks has contributions from gluon fusion ( $gg \rightarrow Q\bar{Q}$ ) and pair annihilation ( $q\bar{q} \rightarrow Q\bar{Q}$ ), which are leading order (LO) processes, while gluon splitting ( $g \rightarrow Q\bar{Q}$ ) and flavor excitation ( $gQ \rightarrow Qg$ ) correspond to processes from the next-to-leading order (NLO). At  $\sqrt{s_{NN}}$  below 10 GeV, the pair creation and flavor excitation processes dominate the heavy quark production, while a negligible contribution is expected from gluon splitting. At the LHC and the highest RHIC energies, the NLO processes domi-

\* [swapneshkhade@gmail.com](mailto:swapneshkhade@gmail.com)

† [ravirathore.physics@gmail.com](mailto:ravirathore.physics@gmail.com)

‡ [yoshini.bailung.1@gmail.com](mailto:yoshini.bailung.1@gmail.com)

§ [ankhi@iiti.ac.in](mailto:ankhi@iiti.ac.in)

nate charm quark production over the LO processes. For beauty quarks, flavor excitation has the highest contribution, while gluon splitting contributes the least among the three production processes. This change in the contribution from different NLO production processes can be attributed to an increase in available phase space in the initial and final state showers as a function of the center of mass energy. The contrast of these contributions shows sensitivity to the quark transverse momentum ( $p_T$ ) as well its pseudo-rapidity ( $\eta$ ) [14, 21, 22].

Parton distribution functions are extracted using global analysis of data obtained from ep, pp, and p-Pb collision systems. Free proton PDFs and nuclear PDFs (nPDFs) are the two types of PDFs that are possible to obtain from data. Nuclear PDFs are modified free proton PDFs due to the EMC effect [23], shadowing, and anti-shadowing in the presence of a nuclear environment. Many free proton PDFs and nPDFs extracted by various groups are available in the LHAPDF database. ATLAS measured the nuclear modification factor of heavy flavors in p-Pb collisions at  $\sqrt{s_{NN}} = 5.02$  TeV, and 8.16 TeV, at forward rapidities [24, 25], revealing the impact of nuclear shadowing at low  $p_T$ . These results are consistent with predictions made using nPDFs [26, 27]. A comparison of rapidity( $y$ ) integrated  $W^\pm/Z$ -boson production by ATLAS [28] and ALICE [29] with theoretical predictions using nPDFs show a  $3.4\sigma$  deviation from free proton PDFs [3]. This emphasizes the significance of nuclear PDFs in heavy-ion collisions, particularly at forward rapidities. We anticipate that heavy quark production will be particularly sensitive to the employment of nPDFs in heavy-ion collisions due to the lower factorization scales involved in production compared to  $W^\pm/Z$  bosons.

In heavy-ion collisions, measurements of heavy flavor nuclear modification factor ( $R_{AA}$ ) [30–35] and elliptic flow ( $v_2$ ) of prompt and non-prompt charm hadrons [36–40] have provided ample information about energy loss mechanisms and thermalization of heavy quarks in the QGP. The measurement of charm  $v_2$  as a function of  $p_T$  by ALICE [36, 39, 40], quotes their participation in the collective medium, corresponding to its thermalization in the region  $2 < p_T < 8$  GeV/ $c$ . Although this measurement confirms the thermalization of charm quarks in the QGP, it cannot comment on the degree of thermalization viz. fraction of thermalized charm quarks. The azimuthal angular correlation of  $D^0 - \bar{D}^0$  can be an excellent observable in this regard, which will allow one to look for effects of thermalization in differential  $p_T$  ranges. The azimuthal angular correlation [41–47], is the distribution of the differences in azimuthal angles,  $\Delta\varphi = \varphi_{\text{trig}} - \varphi_{\text{assoc}}$ , and pseudorapidities,  $\Delta\eta = \eta_{\text{trig}} - \eta_{\text{assoc}}$ , where  $\varphi_{\text{trig}}$  ( $\eta_{\text{assoc}}$ ) and  $\varphi_{\text{trig}}$  ( $\eta_{\text{assoc}}$ ) are the azimuthal angles (pseudorapidities) between the trigger <sup>1</sup> and associated particles <sup>2</sup>, respec-

tively. The correlation function usually contains a “near-side” (NS) peak and an “away-side” (AS) peak at  $\Delta\varphi = 0$  and  $\Delta\varphi = \pi$  respectively over a wide range of  $\Delta\eta$ . For fully thermalized charm quarks, the flight direction will be completely randomized leading to flat  $D^0 - \bar{D}^0$  azimuthal angular correlation [48], and any deviation from flatness can be used to estimate the degree of thermalization. Besides thermalization,  $D^0 - \bar{D}^0$  and  $B - \bar{B}$  azimuthal angular correlation is an excellent probe of heavy flavor production mechanisms. The LO processes are important for the AS peak, while the NLO process like gluon splitting is a major contributor to the NS of  $D^0 - \bar{D}^0$  correlation. A  $p_T$  dependent study will allow disentangling the contribution of pair creation and gluon splitting processes in charm production, and comment on the degree of thermalization.

The ALICE3 experiment investigates the thermalization of charm quarks by measuring the azimuthal angular correlation of  $D^0 - \bar{D}^0$  [48]. In this contribution, we study the effects of nPDFs on the azimuthal angular correlation of prompt  $D^0 - \bar{D}^0$ ,  $B - \bar{B}$ , and non-prompt  $D - \bar{D}$  in Pb-Pb collisions at  $\sqrt{s_{NN}} = 5.5$  TeV. We use the PYTHIA8+Angantyr model [49, 50] to study non-collective effects and provide an effective comment on heavy quark thermalization in heavy ion collisions. Because PYTHIA8 lacks a thermal medium, it is an ideal platform to isolate and study the effects of nPDFs, and make conclusive remarks about the thermalization of heavy flavors. Since nPDFs can affect the production of heavy quarks during initial and final state radiations (ISR and FSR) via hard scatterings, their imprints can reflect in the azimuthal angular correlation of open charm and beauty mesons. The comparison of yields obtained from azimuthal angular correlation of  $D^0$  and  $B$  mesons can give us flavor-dependent and  $p_T$ -dependent relative contributions of gluon splitting and pair creation processes. For non-prompt  $D$ -mesons, these calculations will serve as a proxy for beauty quarks and allow the investigation of different decay-kinematic effects.

This article is organized as follows, In Section II, we briefly discuss about parton distribution function. Section III contains a detailed discussion of the event generation, methodology, and analysis strategy. Section IV includes the results of the study. This section is divided into three subsections for prompt  $D^0 - \bar{D}^0$ ,  $B - \bar{B}$ , and non-prompt  $D - \bar{D}$  azimuthal angular correlations respectively. Important findings of the study are summarized in section V.

## II. PARTON DISTRIBUTION FUNCTION

Parton distribution functions play a pivotal role in hadron and particle physics, as they are crucial for interpreting experimental data from various high-energy processes. PDFs cannot be derived from first principles; instead, they are obtained by comparing theoretical calculations of hadronic cross-sections with experimental

<sup>1</sup> reference particle with respect to which correlation is computed.

<sup>2</sup> particles being correlated with the trigger.

data. These functions are modeled using fit parameters optimized through data to achieve matching theoretical predictions. At an input interaction scale  $Q_0^2$  of partons, PDFs are parameterized for each parton via the equation:

$$f^p(x, Q_0^2) = \mathcal{N} x^{\alpha_f} (1-x)^{\beta_f} \mathcal{I}(x; a) \quad (2)$$

where  $x$  is the Bjorken variable,  $\alpha_f$  and  $\beta_f$  [51] are parameters obtained from data in global QCD analyses. The factor  $\mathcal{N}$  is a normalization constant that accounts for theoretical constraints. The function  $\mathcal{I}(x; a)$ , depending on the set parameters “ $a$ ”, is designed to interpolate between small and large  $x$ -values. The power-like factors  $x^{\alpha_f}$  and  $(1-x)^{\beta_f}$  describe the low- $x$  and high- $x$  behavior of PDFs, inspired by Regge theory [52] and the Brodsky-Farrar quark counting rules [53], respectively.

As previously mentioned, the parameterization of PDFs is set at an input scale  $Q_0$ ; these PDFs subsequently evolve to the scale of data  $Q$  using the DGLAP equation [54–57]. Predictions for hadronic cross-sections are obtained by convoluting the evolved parton distribution functions with partonic cross-sections at a given perturbative order. Optimal PDF parameters are found using a suitable optimization method, commonly the log-likelihood or  $\chi^2$  minimization technique.

Nuclear PDFs are defined as the average of proton and neutron densities in a nucleus [58, 59]:

$$f^{(A,Z)}(x, Q^2) = \frac{Z}{A} f^{p/A}(x, Q^2) + \frac{(A-Z)}{A} f^{n/A}(x, Q^2) \quad (3)$$

In this expression,  $A$  is the atomic mass number,  $Z$  is the atomic number, and  $f^{p,n/A}$  are the proton and neutron-bound PDFs, related to the nucleon PDFs by

$$f^{p,n/A}(x, Q^2) = R_f^A(x, Q^2) f^{p,n}(x, Q^2) \quad (4)$$

where  $R_f^A(x, Q^2)$  is a scale-dependent nuclear modification. This factor illuminates the various nuclear modifications concerning the free proton in different  $x$  regions. A shadowing behavior ( $R < 1$ ) in the low  $x \leq 0.1$  area has been observed in experimental data. This is followed by anti-shadowing ( $R > 1$ ) around  $x \approx 0.1$  and the EMC effect ( $R < 1$ ) in the valence region,  $x \approx 0.4$  [23]. The mechanisms generating these effects are still under investigation but appear as a general feature in all nuclear PDFs.

The free proton PDFs under our consideration are NNPDF2.3 [60] and CT18Anlo [61] PDF. The NNPDF2.3 is a default proton PDF for which different PYTHIA8 processes are tuned, providing a standard PYTHIA8 baseline for comparison. It is the first global PDF set to systematically include all relevant LHC data up to 2012, employing a variable flavor number scheme based on FONLL [62] for heavy quarks. The CT18 QCD global fit uses high-statistics LHC datasets, HERA I + II DIS data, and datasets from the CT14 global QCD analysis [63], totaling 40 datasets. The global fit also incorporates ATLAS  $\sqrt{s} = 7$  TeV  $W$  and  $Z$  boson data.

For CT18Anlo, heavy quarks are parameterized using the SACOT- $\chi$  scheme [64].

The nuclear PDFs used are EPPS21 [65] and nNNPDF3 [66]. The EPPS21 nuclear PDF is derived using CT18nlo as the free proton PDF, with nuclear modifications parameterized at the charm pole mass threshold  $Q_0 = m_{\text{charm}} = 1.3$  GeV. This parameterization addresses the EMC effect, anti-shadowing, and shadowing at appropriate  $x$  values. The number of free parameters in this system is six, and heavy quarks are treated using the SACOT- $\chi$  scheme. The nNNPDF3 uses Machine Learning to extract PDFs from the data, based on NNPDF4 [67] as the free proton PDF, with heavy quarks treated using the FONLL scheme. The use of nNNPDF3.0 is important for examining the effects of different heavy quark treatments.

The above-mentioned PDFs were selected for study due to differences in the theoretical treatment of heavy quarks, the number of fit parameters, the methods used for parameterization, and various other factors.

### III. EVENT GENERATION AND ANALYSIS METHODOLOGY

#### A. The Angantyr model

The PYTHIA8 event generator [49, 50, 68–73] is used to investigate pp, ep, p-A, and A-A collisions in depth. It uses  $2 \rightarrow 2$  QCD matrix elements calculated with leading-order accuracy, incorporating next-to-leading order effects during the parton showering stage. Leading-logarithmic  $p_T$  ordering governs the parton showering, and an extra veto prevents soft-gluon emission divergences. The hadronization process is managed using the Lund string-fragmentation model. It offers a plethora of processes and tunes to use based on the physics involved in the study. PYTHIA8 employs an initial hard scattering with the incoming proton beams, followed by ISR, multi-parton interactions (MPI) [74–76] and FSR processes, comprising the underlying event. The high  $p_T$  partons create showers or jets that fragment and hadronize based on the Lund string fragmentation model [77]. Hadronization is accomplished through the Color Reconnection (CR) mechanism between fragmenting partons [78–81], which is accomplished by rearranging the strings between them. This affects hadronization by modifying the total string length. When the string length is small enough after the subsequent creation of quark-antiquark combinations, the partons hadronize into hadrons. The MPI and CR phenomena in PYTHIA8 play an essential role in the particle production, as evidenced by the charged-particle multiplicity and  $p_T$  distributions, and particle ratios for pp collisions at LHC energies [82].

In PYTHIA8, heavy-flavors are produced via leading order perturbative scattering processes such as gluon fusion ( $gg \rightarrow Q\bar{Q}$ ) or pair annihilation ( $q\bar{q} \rightarrow Q\bar{Q}$ ).

PYTHIA8 approximates higher-order contributions inside its LO framework via flavor excitations ( $gQ \rightarrow Qg$ ) or gluon splittings ( $g \rightarrow Q\bar{Q}$ ) that give rise to heavy-flavor generation during high  $p_T$  parton showers [14, 15].

In PYTHIA8, heavy-ion collisions are simulated using the Angantyr model [50], which extrapolates proton-proton (pp) collision dynamics to nucleus-nucleus (AA) collisions. This generalization is achieved as follows. The positions of nucleons within the nucleus are determined by generating a nuclear density distribution using Monte Carlo methods. The Glauber formalism, which employs the eikonal approximation in impact parameter space, is used to calculate the number of interacting nucleons and binary collisions. In this case, projectile nucleons are supposed to travel in straight lines, colliding with nucleons in the target several times. The contribution from individual nucleon-nucleon interactions in the final state is estimated using the Fritiof model, which accounts for both diffractively and non-diffractively wounded nucleons and manages soft particle production [83]. Hard particles are produced in individual nucleon-nucleon sub-collisions. At high energies, hard partonic sub-collisions play a crucial role, which is addressed by introducing the concepts of primary and secondary absorptive interactions. For both absorptive and diffractive interactions, PYTHIA8 generates the relevant nucleon-nucleon parton-level events utilizing the entire multi-parton interaction (MPI) machinery.

While the Angantyr model does not employ a thermalized medium, it accurately describes the multiplicity of heavy-ion collisions as a function of centrality and  $y$  distribution. As a result, Angantyr offers the unique opportunity to categorize the collective and non-collective effects in heavy-ion collisions. As  $D^0 - \bar{D}^0$  correlation measurements are sensitive to heavy quark thermalization and its participation in the QGP for  $p_T$  ranges from 2 – 6 GeV/ $c$ , our study will allow separating the non-collective components of heavy-flavor production and dynamics in heavy-ion collisions.

## B. Methodology

In addition to the default proton PDF in PYTHIA8, we append LHAPDF6 to access the recent CT18Anlo [61] proton PDF and the EPPS21nlo and nNNPDF3 nuclear PDFs. To establish the effect of nPDFs, we examine the production of  $Z$ -boson as a function of  $y$ . We deploy EPPS21, and nNNPDF3.0, which are modified free proton PDFs in the presence of a nuclear environment. In FIG 1, the ratio between these two PDF settings is compared with the  $Z$ -boson production data from the ATLAS [28] and ALICE [29] experiments. To produce  $Z$ -bosons, weak processes were enabled using `WeakSingleBoson:all=ON`, `WeakDoubleBoson:all=ON`, and `WeakBosonAndParton:all=ON`. The  $y$  dependence also shows that at large rapidities nuclear PDFs provide a better description of experimental data than free proton

PDF calculations.

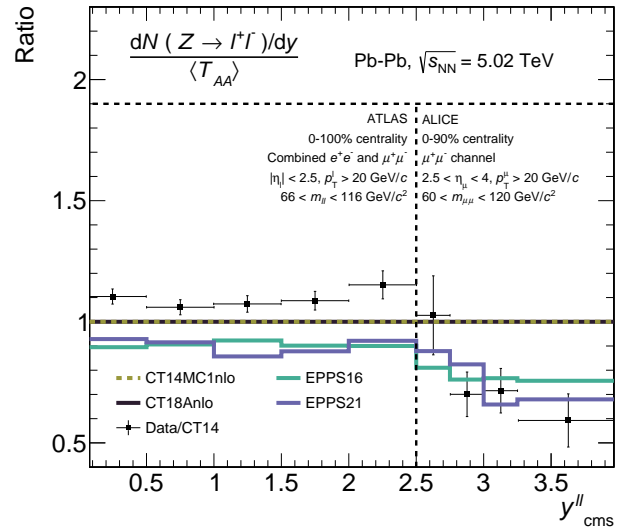


FIG. 1. The ratio of  $Z$ -boson yield (black points) as a function of rapidity measured by ALICE [29] and ATLAS [28] in Pb-Pb collisions at  $\sqrt{s} = 5.02$  TeV to free-nucleon PDF (CT14). The ratios are compared to predictions using different free proton PDFs (CT14MC1nlo, CT18nlo) and nuclear PDFs (EPPS16, EPPS21).

We generate  $\sim 1$ B events for each PDF in Pb-Pb collisions at  $\sqrt{s_{NN}} = 5.5$  TeV. Heavy-flavor hadrons are selected by maintaining the ALICE3 acceptance of  $|y| < 4.0$ . The non-diffractive component of the total cross-section for all soft QCD processes is used with the switch `SoftQCD: Non-diffractive=on` with MPI, ISR, and FSR to simulate minimum bias events. In the case of prompt  $D^0 - \bar{D}^0$ , the correlation distribution was obtained by correlating  $D^0$  and  $\bar{D}^0$  coming from the same hard scattering. This is ensured by tracing the produced (anti-)charm quark until it hadronizes to  $(\bar{D}^0)D^0$ , through its decay daughter at each stage of fragmentation. To ensure they come from the same scattering, the mothers of  $c$  and  $\bar{c}$  are matched. The same procedure is repeated for  $B - \bar{B}$  meson correlation, but in this case, all B-meson species are used as trigger particles instead of just  $B^0$ . In the case of non-prompt  $D^0, D^+, D_s^+$ , and their antiparticles, we trace the  $b$  quark until it decays to one of the D-meson species. Later, the mothers of  $b$  and  $\bar{b}$  are checked to ensure they come from the same scattering.

The prompt  $D^0 - \bar{D}^0$  correlation distribution is fitted with two generalized Gaussian functions for the NS peak<sup>1</sup>, a Gaussian function for the AS peak, and a 0<sup>th</sup>

<sup>1</sup> The two generalized Gaussians are used to estimate the double peak structure forming at the NS.

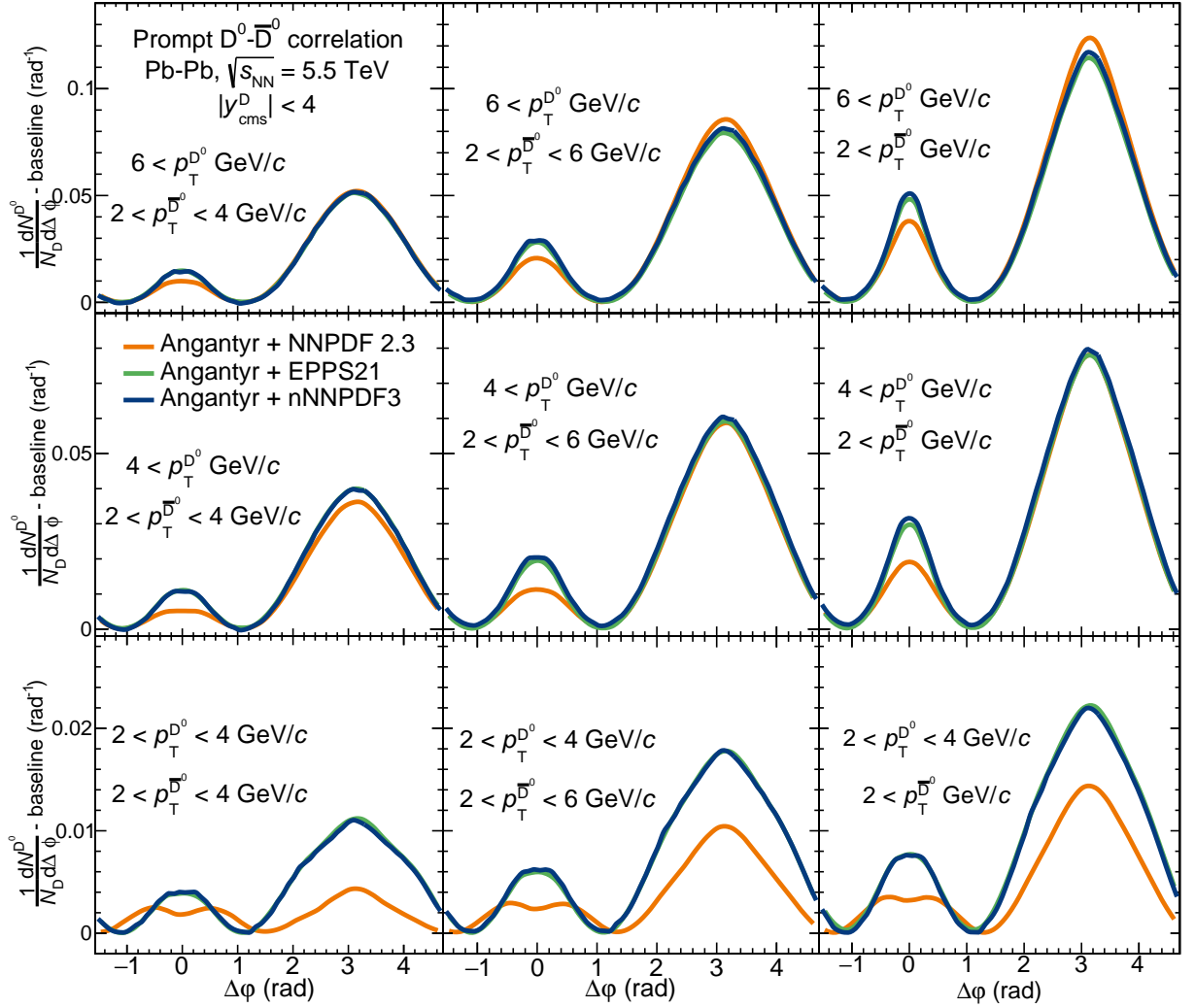


FIG. 2. Comparison of azimuthal angular correlations of prompt  $D^0 - \bar{D}^0$  mesons originating from the same hard scattering process, using free parton distribution functions (NNPDF2.3) and nuclear parton distribution functions (EPPS21, nNNPDF3), simulated with PYTHIA8+Angantyr at  $\sqrt{s} = 5.5$  TeV is shown for different  $p_T^{\text{trig}}$  and  $p_T^{\text{assoc}}$  ranges.

order polynomial for the baseline identification given as

$$f(\Delta\phi) = b + \sum_{i=1}^2 \frac{Y_{\text{NS}_i} \times \beta_{\text{NS}_i}}{2\alpha_{\text{NS}_i} \Gamma(1/\beta_{\text{NS}_i})} \times e^{-\left(\frac{\Delta\phi}{\alpha_{\text{NS}_i}}\right)^{\beta_{\text{NS}_i}}} + \frac{Y_{\text{AS}}}{\sqrt{2\pi}\sigma_{\text{AS}}} \times e^{-\left(\frac{\Delta\phi - \pi}{\sqrt{2}\sigma_{\text{AS}}}\right)^2}. \quad (5)$$

Here,  $Y_{\text{NS}}$  and  $Y_{\text{AS}}$  are the yields of NS and AS peaks,  $\beta_{\text{NS}}$  is called shape parameter for the near-side peak, and  $\alpha_{\text{NS}}$  is related to the  $\sigma_{\text{NS}}$  (width) of the peak as

$$\sigma_{\text{NS}} = \alpha_{\text{NS}} \sqrt{\Gamma(3/\beta_{\text{NS}})/\Gamma(1/\beta_{\text{NS}})} \quad (6)$$

The non-prompt D-meson correlation distribution is fitted with a single generalized Gaussian function for the NS peak, von Mises for the AS peak, and a 0<sup>th</sup> order

polynomial for the baseline identification given by

$$f(\Delta\phi) = b + \frac{Y_{\text{NS}} \times \beta_{\text{NS}}}{2\alpha_{\text{NS}} \Gamma(1/\beta_{\text{NS}})} \times e^{-\left(\frac{\Delta\phi}{\alpha_{\text{NS}}}\right)^{\beta_{\text{NS}}}} + \frac{e^{\kappa_{\text{AS}} \cos(\Delta\phi - \pi)}}{2\pi I_0(\kappa_{\text{AS}})} \quad (7)$$

where  $b$  is the baseline,  $\kappa$  is the reciprocal measure of dispersion that quantifies the width of the distribution,  $I_0$  is the 0<sup>th</sup> order modified Bessel function. The mean of the AS peak is fixed at  $\Delta\phi = \pi$ . The NS width is obtained in a similar manner as prompt  $D^0$ , but the AS width is estimated by calculating the sigma ( $\sigma$ ) from the von Mises function as per the given relation:

$$\sigma = \sqrt{-2 \log \frac{I_1(\kappa)}{I_0(\kappa)}} \quad (8)$$

Here,  $I_0$  and  $I_1$  are the modified Bessel functions of 0<sup>th</sup>

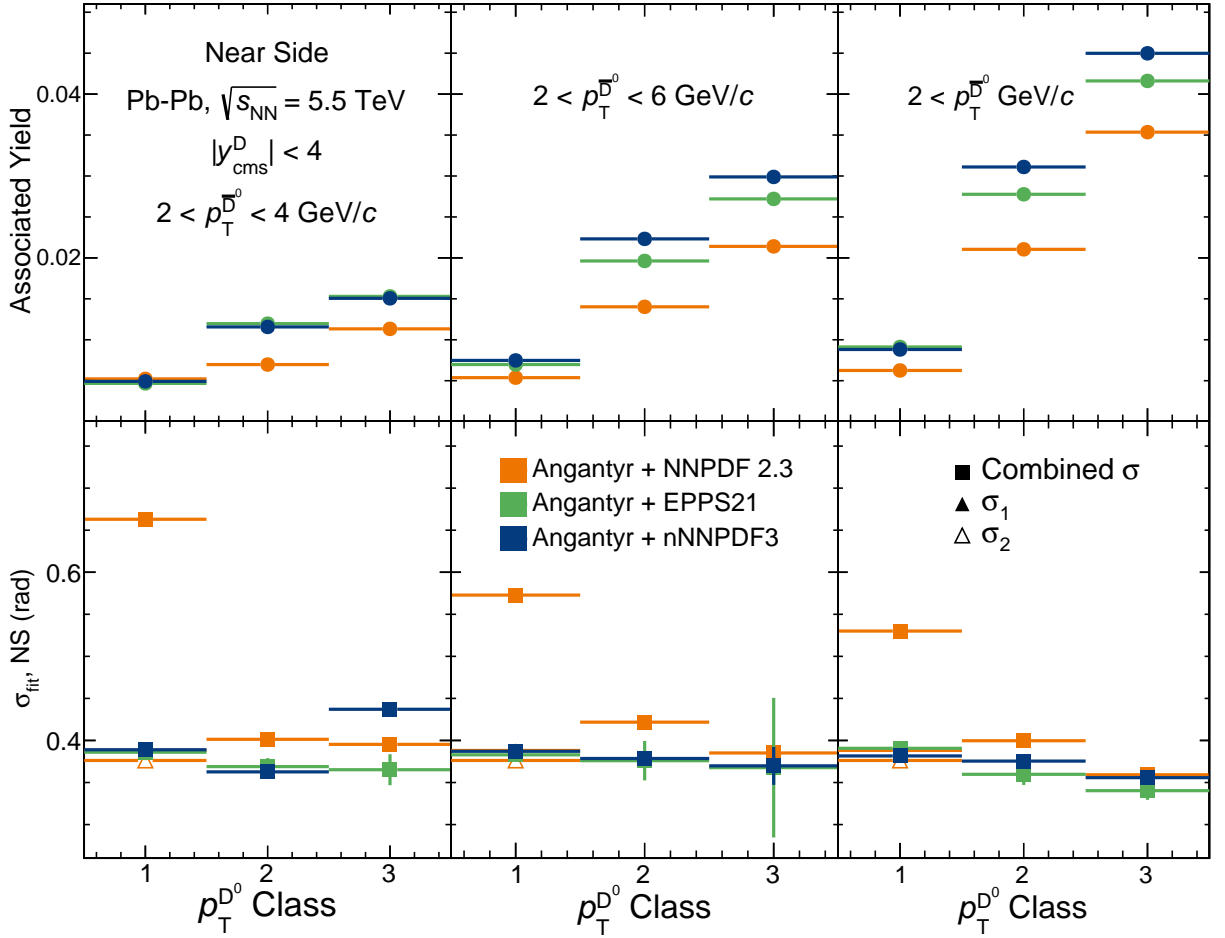


FIG. 3. Comparison of near-side yield (top row) and width (bottom row) of azimuthal angular correlation of  $D^0 - \bar{D}^0$  meson using free parton distribution functions (NNPDF2.3) and nuclear parton distribution functions (EPPS21, nNNPDF3), simulated with PYTHIA8+Angantyr at  $\sqrt{s} = 5.5$  TeV. Triangular markers (hollow and filled) for  $p_T^{\text{trig}}$  class I represent individual widths of two peaks, and square marker represents combined width.

and 1<sup>st</sup> order, respectively, and  $\kappa$  is measured by the von Mises function fit parameter. The error in the width ( $d\sigma$ ) is propagated by the relation:

$$d\sigma = \frac{1}{\sigma} \left( \frac{I_1}{I_0} - \frac{I_0}{I_1} + \frac{1}{\kappa} \right) d\kappa \quad (9)$$

where  $d\kappa$  is the uncertainty in  $\kappa$ , obtained from the fit result.

In the case of  $B - \bar{B}$ , the AS peak exhibits a Gaussian-like structure for low associated  $p_T$  ranges, while a triangular nature for high associated  $p_T$  ranges, which inspired us to develop a novel function for the away-side peak. The  $B - \bar{B} \Delta\phi$  distribution is fitted with two generalized Gaussian functions for the NS peak, the convolution of a Gaussian function and a triangular function for the AS peak, and a 0<sup>th</sup> order polynomial for the baseline identification given by

$$f(\Delta\phi) = b + \sum_{i=1}^2 \frac{Y_{\text{NS}_i} \times \beta_{\text{NS}_i}}{2\alpha_{\text{NS}_i} \Gamma(1/\beta_{\text{NS}_i})} \times e^{-\left(\frac{\Delta\phi}{\alpha_{\text{NS}_i}}\right)^{\beta_{\text{NS}_i}}} + (a - |\Delta\phi - \pi|) \frac{Y_{\text{AS}}}{\sqrt{2\pi}\sigma_{\text{AS}}} \times e^{-\left(\frac{\Delta\phi - \pi}{\sqrt{2}\sigma_{\text{AS}}}\right)^2} \quad (10)$$

Here, the away-side mean is fixed at  $\Delta\phi = \pi$ , and the parameter “ $a$ ” is responsible for the shape of the distribution. For small values of “ $a$ ”, the AS function behaves like a Gaussian, while for large values of “ $a$ ”, it becomes triangular. The width of the AS distribution is extracted from its standard deviation.

The choice of fitting function for the three heavy flavors is based on the reduced- $\chi^2$  of the fit that best describes the shape of the obtained  $\Delta\phi$  correlations.

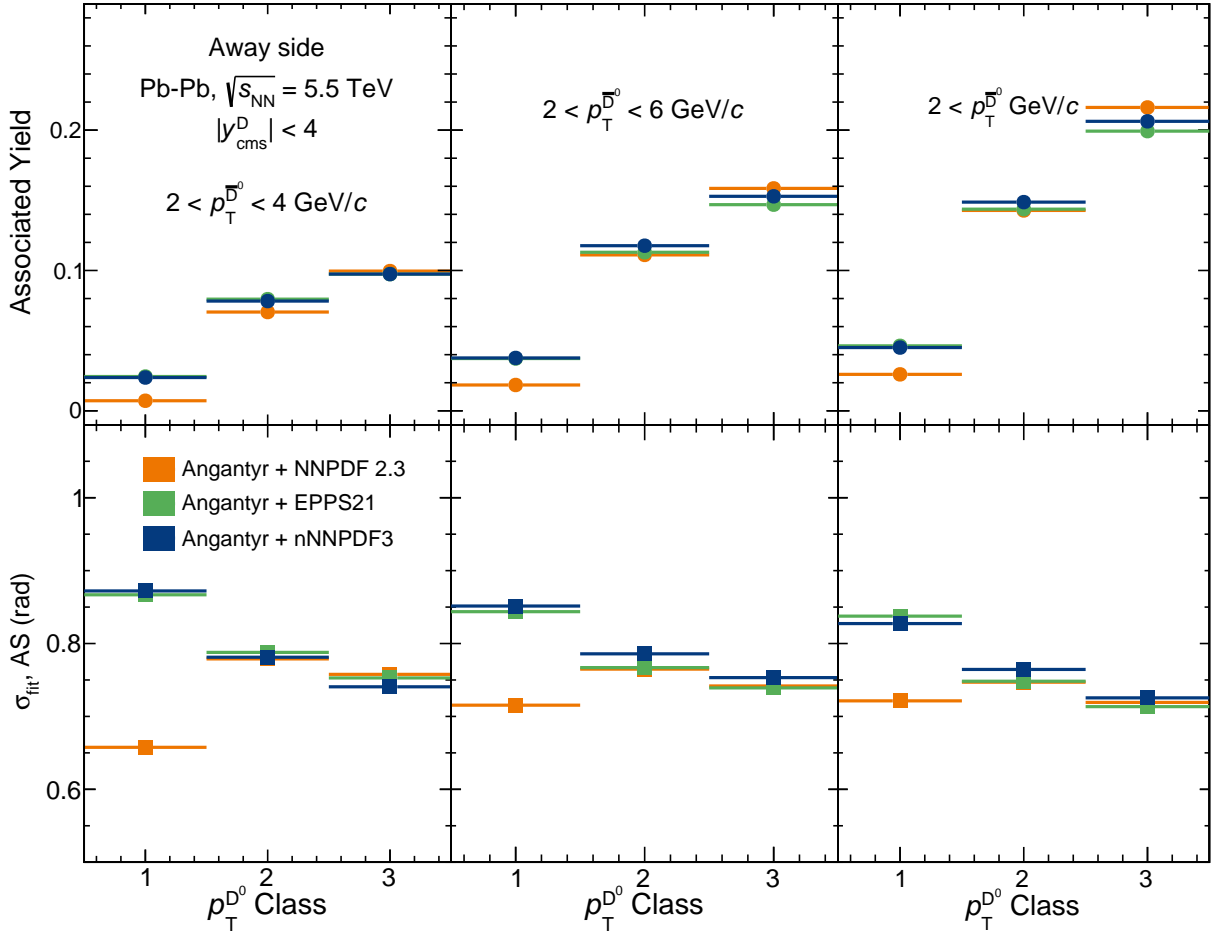


FIG. 4. Comparison of away-side yield (top row) and width (bottom row) of azimuthal angular correlation of  $D^0 - \bar{D}^0$  meson using free parton distribution functions (NNPDF2.3) and nuclear parton distribution functions (EPPS21, nNNPDF3), simulated with PYTHIA8+Angantyr at  $\sqrt{s} = 5.5$  TeV.

#### IV. RESULTS

##### A. $D^0 - \bar{D}^0$ azimuthal angular correlation

The azimuthal angular correlation of  $D^0 - \bar{D}^0$  using NNPDF2.3, EPPS21, and nNNPDF3 for different triggers and associated  $p_T$  ranges is shown in FIG 2. The trigger particles are classified into 3 classes with  $p_T^{\text{trig}}$  ranges  $2 - 4$ ,  $\geq 4$ , and  $\geq 6$  GeV/c, while associated particles are selected in the  $p_T^{\text{assoc}}$  ranges of  $2 - 4$ ,  $2 - 6$ ,  $2 - 50$  GeV/c. FIG 3 and FIG 4 provide a quantitative comparison of NS and AS yields and widths of the  $\Delta\varphi$  distribution, respectively. Key observations from prompt  $D^0 - \bar{D}^0$  correlations are as follows:

1. The NS and AS peaks of the  $D^0 - \bar{D}^0$  azimuthal angular correlation function for EPPS21 and nNNPDF3 are qualitatively similar in all  $p_T^{\text{trig}}$  and  $p_T^{\text{assoc}}$  intervals. In contrast, proton PDF correlations are distinctly different, showing a smaller yield and a double-peak structure at NS, which is unseen for nPDFs.

$p_T^{\text{assoc}}$ (GeV/c)	Mean of near side peaks (rad)		
	$m_1$	$m_2$	$ m_1 - m_2 $
$2 < p_T < 4$	-0.58	0.56	1.14
$2 < p_T < 6$	-0.51	0.46	0.97
$p_T > 2$	-0.43	0.43	0.86

TABLE I. Separation between two near-side peaks for different associated  $p_T$  ranges for trigger range  $2 < p_T^{\text{trig}} < 4$  GeV/c.

2. The angle between produced  $c - \bar{c}$  pairs during the gluon splitting process results in a double-peak structure at the NS. TABLE I shows that the separation between two NS peaks diminishes as the  $p_T^{\text{assoc}}$  range increases for the given  $p_T^{\text{trig}}$  range. The observation can be explained by the fact that, at low  $p_T^{\text{assoc}}$ , the opening angle is wide, while at higher  $p_T^{\text{assoc}}$ , the angle narrows due to a larger initial gluon boost. For  $p_T^{\text{trig}} > 4$  GeV/c, the double NS peak disappears due to insignificant opening angles to resolve the two peaks.

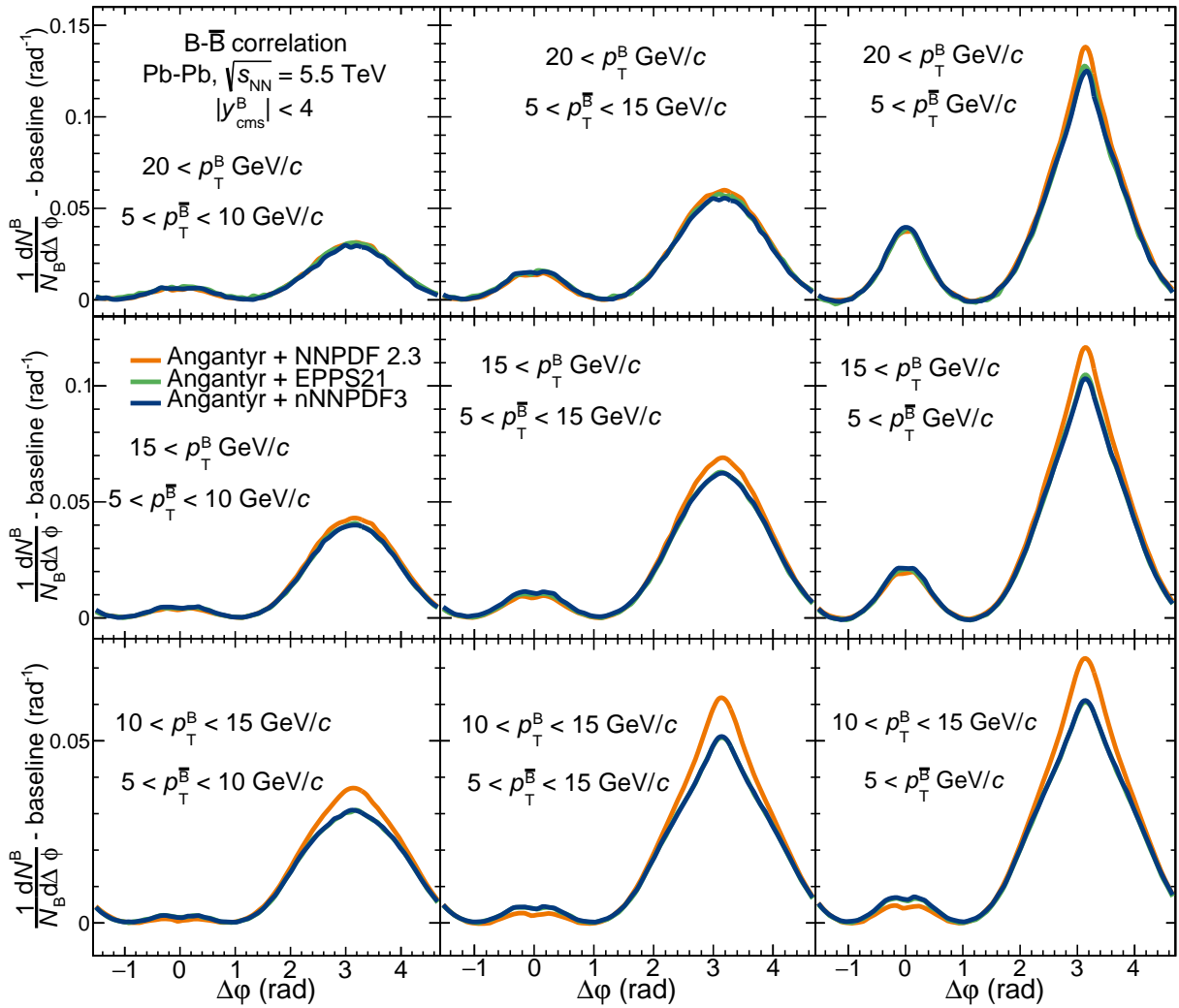


FIG. 5. Comparison of azimuthal angular correlations of prompt  $B - \bar{B}$  mesons originating from the same hard scattering process, using free parton distribution functions (NNPDF2.3) and nuclear parton distribution functions (EPPS21, nNNPDF3), simulated with PYTHIA8+Angantyr at  $\sqrt{s} = 5.5\text{ TeV}$  is shown for different  $p_T^{\text{trig}}$  and  $p_T^{\text{assoc}}$  ranges.

3. FIG 3 shows a quantitative comparison between the width and yield of the NS peak. The lower panel of FIG 3 displays the widths of the two individual NS peaks ( $\sigma_1, \sigma_2$ ) and the combined width ( $\sigma$ ). The individual widths of both peaks using free proton PDFs are consistent with the NS widths using nPDFs. However, the combined width is significantly higher than the yield obtained using the nPDFs. The combined width decreases with the inclusion of high  $p_T^{\text{assoc}}$ , which has a higher initial boost during production, resulting in a narrower opening angle.
4. Quantitatively, FIG 3 shows that for  $p_T^{\text{trig}}$  Class I, the yields using proton PDFs and nPDFs are consistent. A small discrepancy in high  $p_T^{\text{assoc}}$  can be attributed to uncertainties in PDFs and baseline estimation.
5. For  $p_T^{\text{trig}}$  Class II and III, yields obtained using EPPS21 and nNNPDF3.0 are consistent, but the yield obtained using NNPDF2.3 is much lower. As  $p_T^{\text{assoc}}$  grows, the discrepancy between free proton PDF and nPDF calculations rises.
6. For  $p_T^{\text{trig}}$  Class I, the AS width computed using free proton PDFs is much smaller than the widths calculated using nPDFs widths. The difference between widths computed using proton PDF and nPDFs reduces with increasing  $p_T^{\text{assoc}}$  and  $p_T^{\text{trig}}$  ranges. Except at low  $p_T^{\text{assoc}}$ , the AS yield for proton PDFs and nPDFs is consistent.
7. The width of the AS peak also shows a decreasing trend for all ranges of  $p_T^{\text{assoc}}$  and  $p_T^{\text{trig}}$  in the case of nPDFs. This can be due to the increasing boost of associated particles with increasing  $p_T^{\text{assoc}}$  and  $p_T^{\text{trig}}$ .

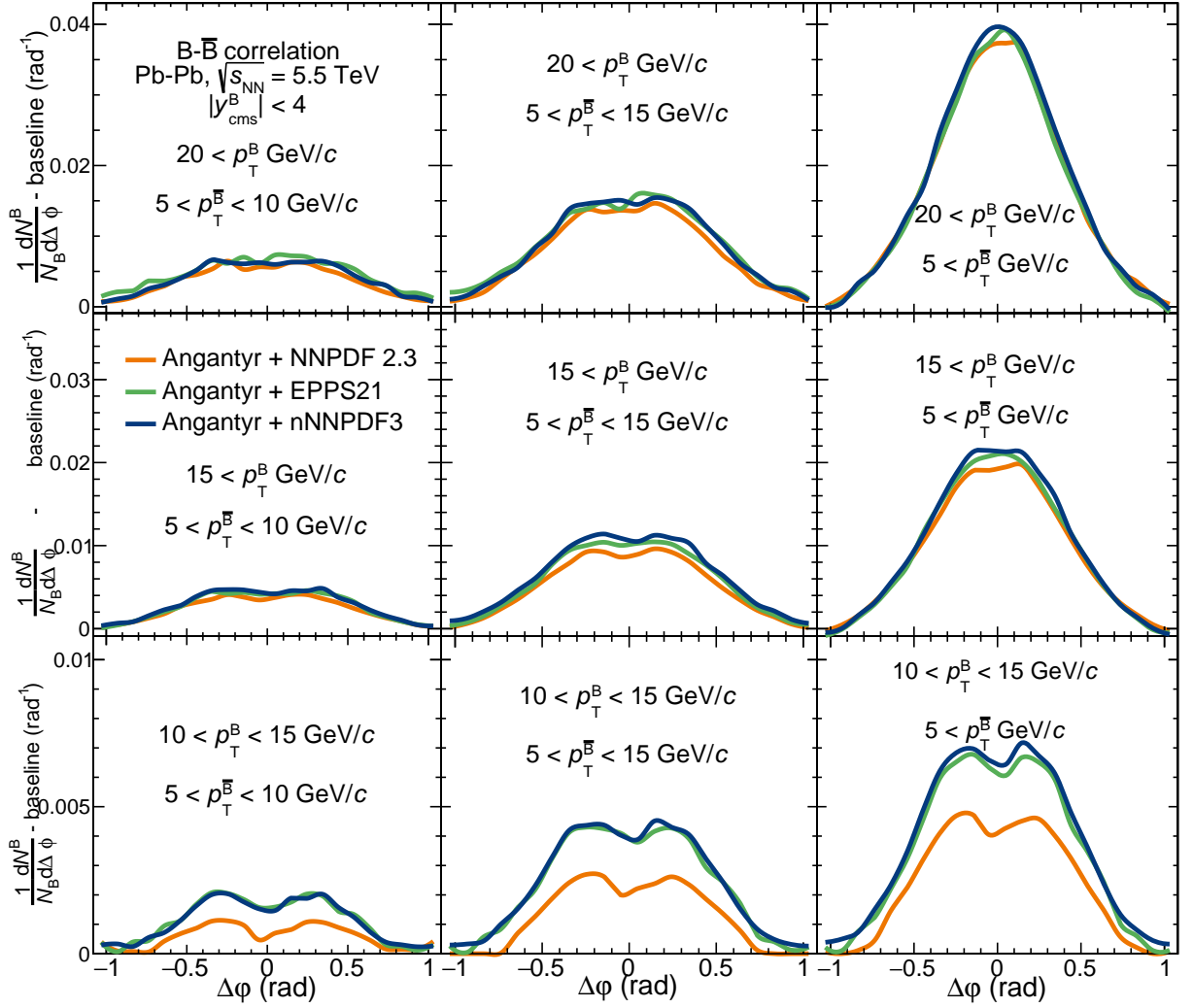


FIG. 6. Comparison of near-side azimuthal angular correlation of  $B - \bar{B}$  meson between free proton parton distribution function (NNPDF2.3) and nuclear PDF (EPPS21, nNNPDF3) with PYTHIA8+Angantyr in Pb-Pb collisions at  $\sqrt{s} = 5.5$  TeV is shown for different  $p_T^{\text{trig}}$  and  $p_T^{\text{assoc}}$  ranges. The near-side peak is plotted for  $|\Delta\phi| = 1$ .

8. FIG 12 indicates that except for  $p_T^{\text{trig}}$  Class I and  $p_T^{\text{assoc}}$  between 2 – 4 GeV/c, NS yields due to nPDFs are always bigger than free proton PDF (more than 30%). NS correlation widths are similar for  $p_T^{\text{trig}}$  Class II and III across different PDFs, however for  $p_T^{\text{trig}}$  Class I widths obtained using PDFs are narrower compared to free proton PDFs (more than 20%). On the other hand, FIG 13 shows that except for  $p_T^{\text{trig}}$  Class I, nPDF NS yields are always smaller than free proton PDF (approximately 50%). AS correlation widths are compatible for  $p_T^{\text{trig}}$  Class II and III among different PDFs, but for  $p_T^{\text{trig}}$  Class I nPDF gives a broader correlation compared to free proton PDFs (more than 15%).
9. The panel with  $p_T^{\text{trig}} > 4$  GeV/c and  $4 > p_T^{\text{assoc}} > 2$  GeV/c is critical for measuring the degree of thermalization of the charm quark, because collec-

tive effects are dominant in this  $p_T$  range. In this range, medium effects can flatten the  $D^0 - \bar{D}^0$  azimuthal angular correlation in actual Pb-Pb collisions. FIG 3 and 4 illustrate that the NS and AS peaks have identical widths within PDF uncertainties. nPDFs have no appreciable impact on the broadening of the azimuthal correlation in this  $p_T$  range for minimum bias Pb-Pb events. Central collisions are likely to provide more intriguing effects.

## B. $B - \bar{B}$ meson azimuthal angular correlation

FIG 5 shows the differential azimuthal angular correlation of  $B - \bar{B}$  across all species of beauty mesons. The  $p_T^{\text{trig}}$  ranges are 10 – 15,  $\geq 15$ , and  $\geq 20$  GeV/c, while the associated particles are picked in the  $p_T^{\text{assoc}}$  ranges 5 – 10, 10 – 15, and  $> 5$  GeV/c. FIG 7 and FIG 8 pro-

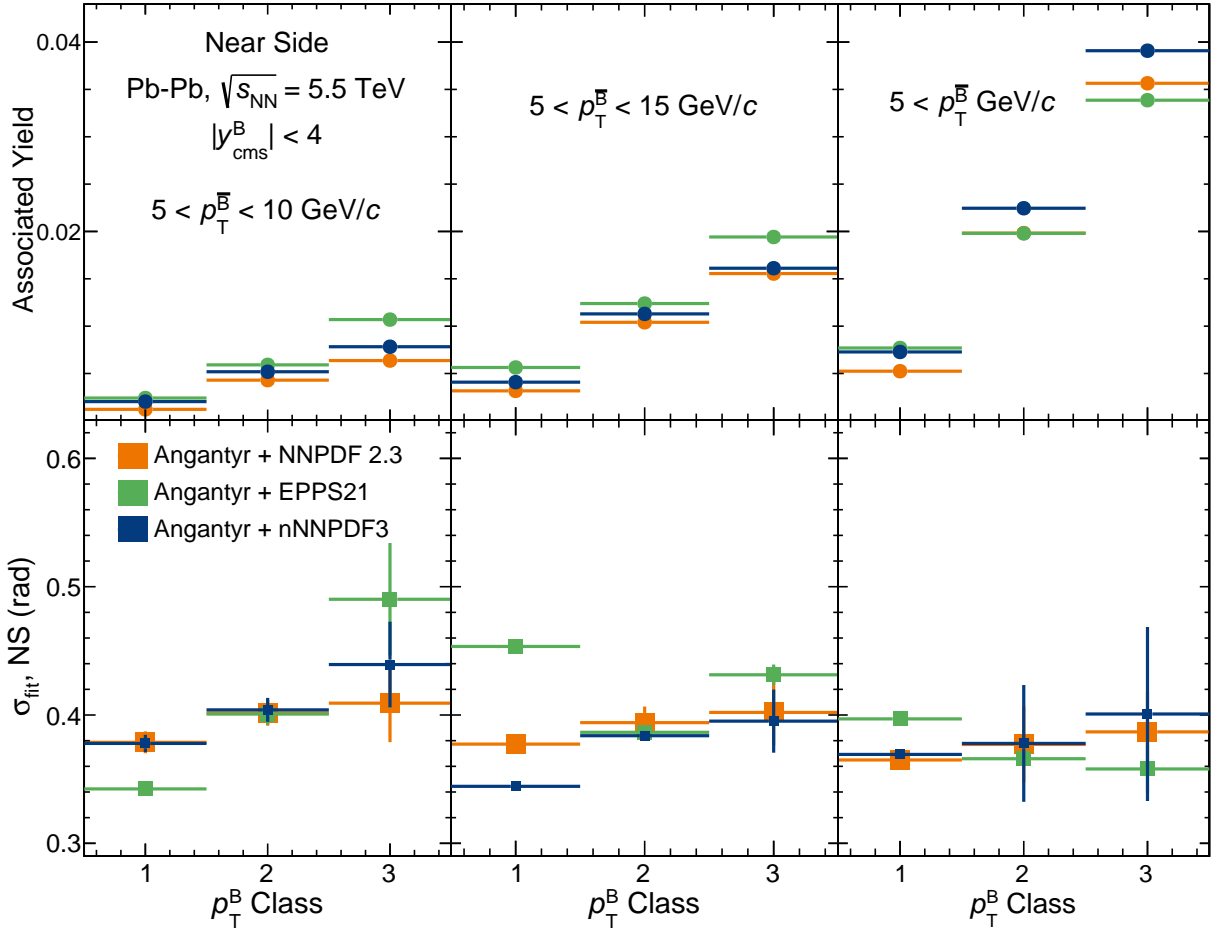


FIG. 7. Comparison of near-side yield (top row) and sigma (bottom row) of azimuthal angular correlation of  $B - \bar{B}$  meson between free proton parton distribution function (NNPDF2.3) and nuclear PDF (EPPS21, nNNPDF3) with PYTHIA8+Angantyr in Pb-Pb collisions at  $\sqrt{s} = 5.5$  TeV for different  $p_T^{\text{trig}}$  and  $p_T^{\text{assoc}}$  ranges.

vide a quantitative comparison of yield and width of the NS and AS peaks of the azimuthal angular distribution, respectively. At low trigger and association  $p_T$  ranges, the away-side distribution (pair creation) dominates the near-side distribution (gluon splitting) due to its broader width. The choice of higher  $p_T$  ranges compared to  $D^0 - \bar{D}^0$  correlation is made to study these features of azimuthal angular correlation arising due to production processes.

1. Qualitatively, the NS azimuthal angular distribution of  $B - \bar{B}$  is consistent with the nPDFs and free proton PDF. The discrepancy between proton PDF and nPDF is observed for the AS peak of correlation for  $p_T^{\text{trig}}$  ranges between  $10 < p_T^{\text{trig}} < 15$  and  $15 < p_T^{\text{trig}}$ . The near side peak of  $B - \bar{B}$  azimuthal correlation is much smaller than the away side peak, this is because the ratio of gluon splitting production cross-section to pair creation cross-section is smaller for beauty quark as compared to charm quark ratio [14].
2. FIG 6 shows the NS angular correlation of  $B - \bar{B}$

between  $-1 < \Delta\phi < 1$  for better visualization. For  $10 < p_T^{\text{trig}} < 15$  GeV/c, two resolved peaks due to gluon splitting are visible. This  $p_T^{\text{trig}}$  range also suggests that correlations from free proton PDF are smaller than for nPDF. All three PDFs give compatible results for the other two  $p_T^{\text{trig}}$  ranges. It can also be observed that the separation between two near-side peaks is reduced after the inclusion of high  $p_T^{\text{assoc}}$  particles due to an increased boost of gluons undergoing splitting. TABLE II quantitatively shows the boost effect due to high  $p_T$  particles on two separating NS peaks.

3. FIG 7 reports the yields of the NS distribution showing an increasing trend as a function of  $p_T^{\text{trig}}$  and  $p_T^{\text{assoc}}$ . Similarly, the AS yield is increasing as a function of  $p_T^{\text{assoc}}$ , but  $p_T^{\text{trig}}$  dependence shows an interesting trend. The yield increases for the first two  $p_T^{\text{trig}}$  classes and decreases for Class III. The difference between Class II and Class III yields decreases after including higher  $p_T$  of  $\bar{B}$ . At the highest  $p_T^{\text{assoc}}$  range, the yield of trigger Class III be-

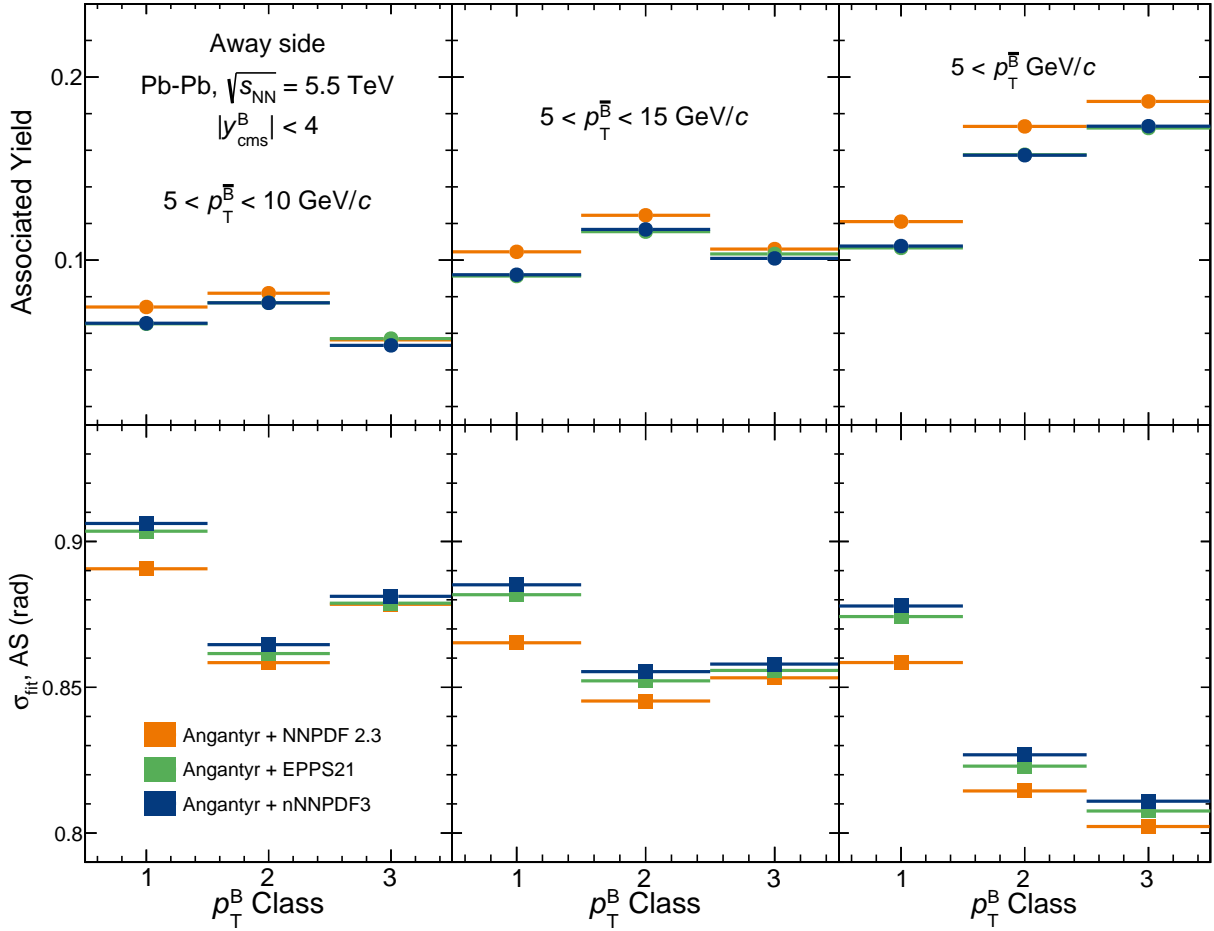


FIG. 8. Comparing away-side yield (top row) and sigma (bottom row) of azimuthal angular correlation of  $B - \bar{B}$  meson between free proton parton distribution function (NNPDF2.3) and nuclear PDF (EPPS21, nNNPDF3) with PYTHIA8+Angantyr in Pb-Pb collisions at  $\sqrt{s} = 5.5$  TeV for different  $p_T^{\text{trig}}$  and  $p_T^{\text{assoc}}$  ranges.

comes greater than Class II. This observation can be explained by considering a non-zero  $\Delta p_T$  between the  $b - \bar{b}$  pair created in initial hard scattering [14], which shows that it is most likely to have associated particles in  $\Delta p_T \approx 3$  GeV/c for pair creation and  $\Delta p_T \approx 5$  GeV/c for gluon splitting. In the AS peak, the small  $\Delta p_T$  range suggests a lesser abundance of associated particles at lower  $p_T$  for high  $p_T^{\text{trig}}$ . Comparable AS yield for Class II and Class III for the  $p_T^{\text{assoc}} > 5$  GeV/c supports this explanation by showing an increasing trend with  $p_T^{\text{trig}}$ . An absence of such observation at the near side is a consequence of a larger  $\Delta p_T$  range for gluon splitting. This effect is observed for all PDFs under consideration.

4. The width of the NS angular distribution does not show any significant  $p_T^{\text{trig}}$  dependence for  $5 < p_T^{\text{assoc}} < 15$  GeV/c and  $5 \text{ GeV/c} < p_T^{\text{assoc}}$  range. On the other hand, the width of the distribution increases as a function of  $p_T^{\text{trig}}$  for  $5 < p_T^{\text{assoc}} < 10$  GeV/c. The increasing trend is observed due to the exclu-

sion of highly correlated high  $p_T$  associated particles caused by the large difference between the  $p_T$  values of the trigger and associated particles. The larger the  $\Delta p_T$  between triggers as associated particles, the strength of the correlation will be weaker, leading to a broader width. This phenomenon also shows its imprints in the trends of AS width, where the width of trigger Class III is higher than trigger Class II. The difference between Class III and Class II width reduces as we include higher  $p_T$  associated particles due to a reduction in  $\Delta p_T$ . FIG 8 and FIG 7 also show that  $p_T^{\text{trig}}$  dependent trends for  $5 < p_T^{\text{assoc}} < 10$  GeV/c are opposite for NS and AS distribution.

5. FIG 12 suggests that NS yields are consistent except for low associated and trigger class. For  $5 < p_T^{\text{assoc}} < 10$  GeV/c, yields obtained using nPDFs is 20% higher than yields obtained using free proton PDFs for  $p_T^{\text{trig}}$  Class II and Class III for nNNPDF and around 40-60% for EPPS21. For  $p_T^{\text{trig}}$  Class I, this ratio is even higher for  $5 < p_T^{\text{assoc}} < 10$  GeV/c.

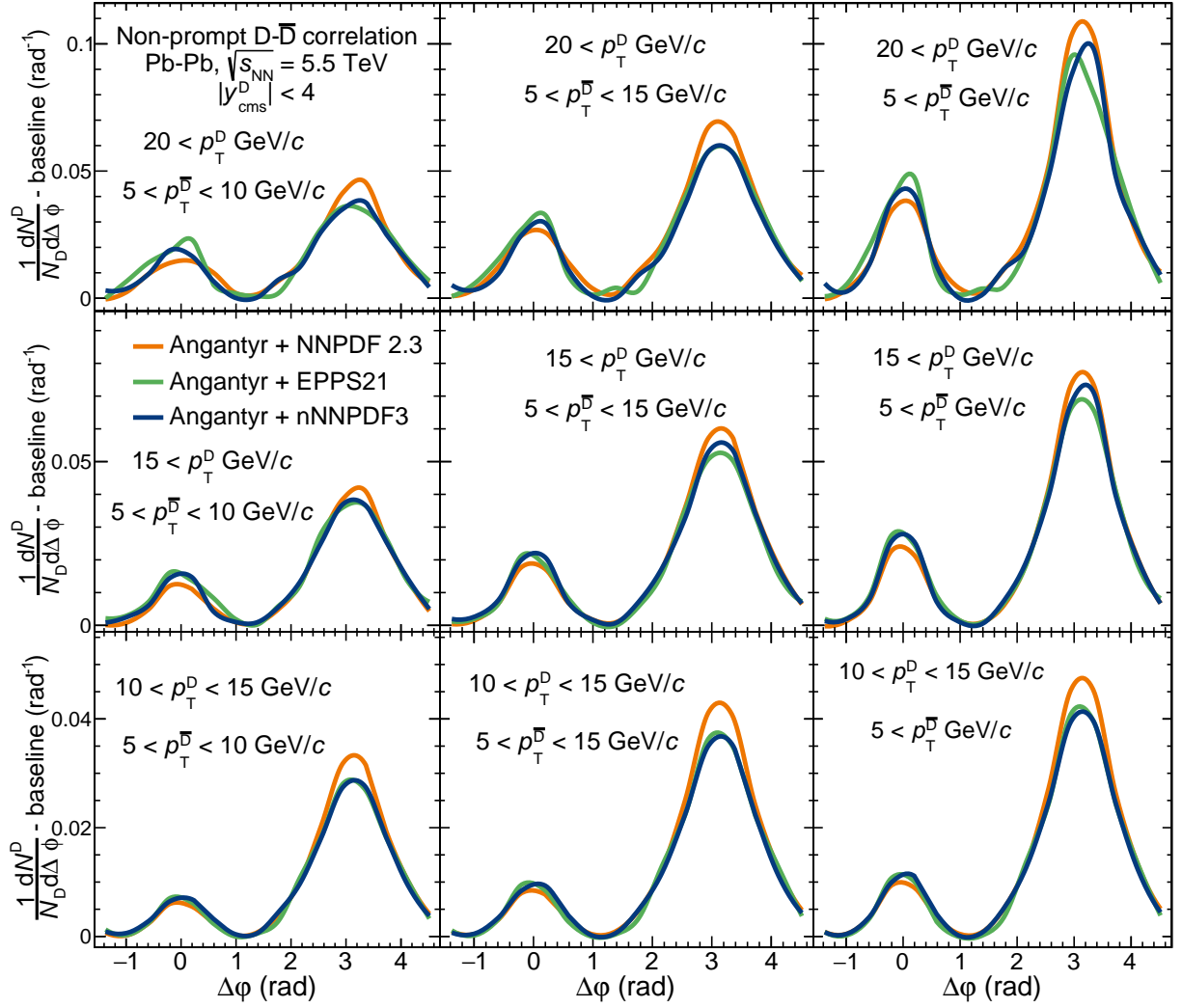


FIG. 9. Comparison of azimuthal angular correlation of non-prompt D –  $\bar{D}$  meson between free proton parton distribution function (NNPDF2.3) and nuclear PDF (EPPS21, nNNPDF3) with PYTHIA8+Angantyr in Pb-Pb collisions at  $\sqrt{s} = 5.5$  TeV.

$p_T^{\text{assoc}}$ (GeV/c)	Mean of near side peaks (rad)			
	Class I	$m_1$	$m_2$	$ m_1 - m_2 $
$5 < p_T < 10$		-0.31	0.31	0.62
$5 < p_T < 15$		-0.3	0.31	0.61
$5 < p_T$		-0.29	0.31	0.60
Class II				
$5 < p_T < 10$		-0.34	0.36	0.70
$5 < p_T < 15$		-0.30	0.30	0.60
$5 < p_T$		-0.30	0.27	0.57
Class III				
$5 < p_T < 10$		-0.29	0.29	0.58
$5 < p_T < 15$		-0.13	0.13	0.26
$5 < p_T$		-0.01	0.02	0.03

TABLE II. Separation between two near-side peaks of B –  $\bar{B}$  azimuthal angular correlation for different associated  $p_T^{\text{trig}}$  and  $p_T^{\text{assoc}}$  ranges.

It is interesting to notice that for  $p_T^{\text{trig}}$  Class I, all associated ranges for both nuclear PDFs give more than 30% higher yield compared to free proton PDF.

- The ratios of NS correlation width are consistent within the uncertainties ( $\approx 20\%$ ) of parton distribution functions used. The AS yield and width ratios are consistent with proton PDF within 10%. No distinct  $p_T^{\text{trig}}$ , as well as  $p_T^{\text{assoc}}$  dependence, is observed; this can be due to higher trigger and associated  $p_T$  ranges compared to  $D^0 - \bar{D}^0$  azimuthal correlations.

### C. Non-prompt D – $\bar{D}$ meson azimuthal angular correlation

Non-prompt D-mesons act as a measurable proxy of B-mesons hence azimuthal angular correlation of non-

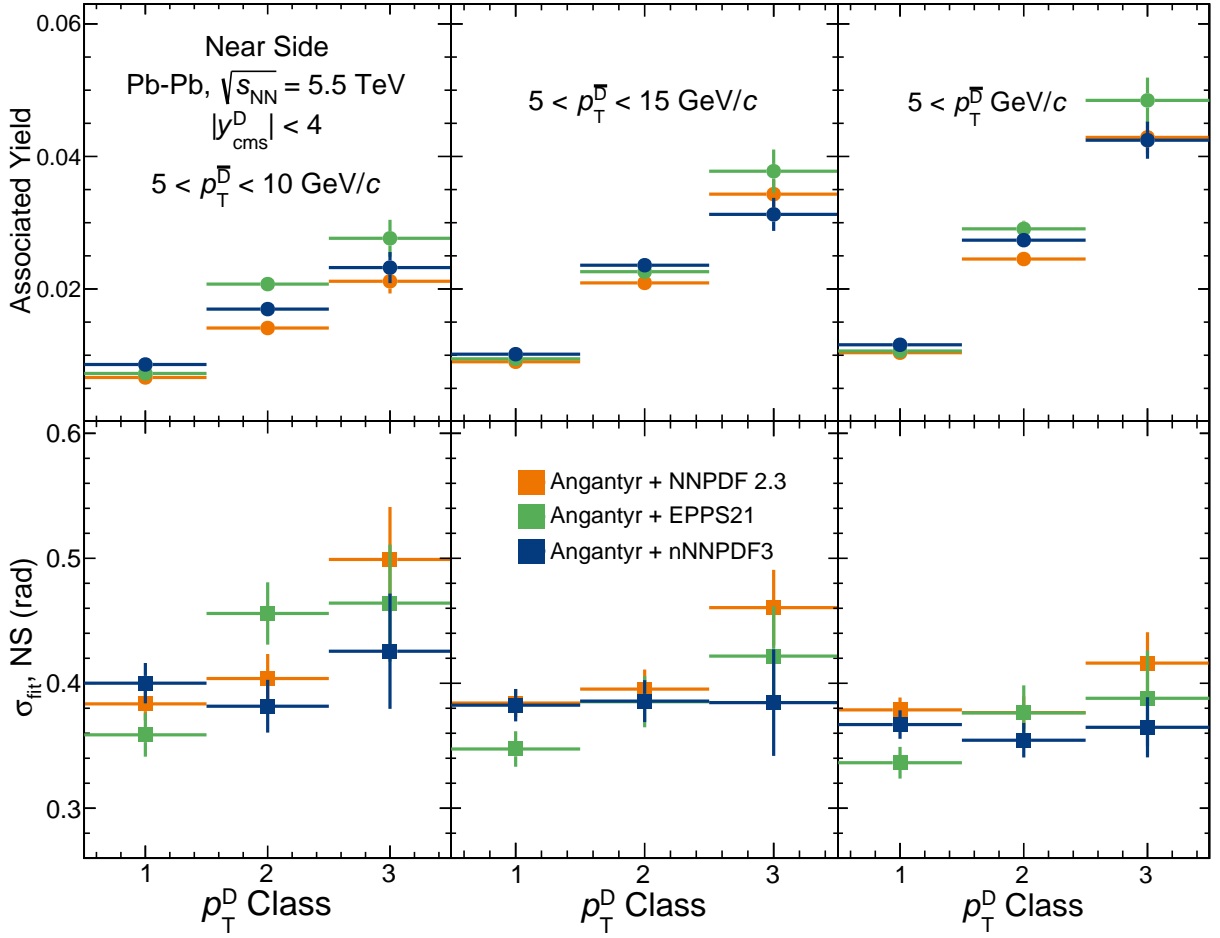


FIG. 10. Comparison of near-side yield (top row) and sigma (bottom row) for azimuthal angular correlation of non-prompt  $D - \bar{D}$  meson between free proton parton distribution function (NNPDF2.3) and nuclear PDF (EPPS21, nNNPDF3) with PYTHIA8+Angantyr in Pb-Pb collisions at  $\sqrt{s} = 5.5$  TeV.

prompt  $D - \bar{D}$  is important to understand the dynamics of beauty quark. FIG 9 shows the  $p_T$  differential azimuthal angular correlation of non-prompt  $D - \bar{D}$  using non-prompt  $D^0, D^+$  and  $D_s^+$  mesons. Trigger  $p_T$  ranges are 10-15,  $\geq 15$ , and  $\geq 20$  GeV/c, while associated particles are selected in the ranges 5-10, 5-20, 5-50 GeV/c. Similar to  $B - \bar{B}$  correlations, the associated particles are selected within  $|\Delta\eta| < 1$ . FIG 10 and FIG 11 provide a quantitative comparison of yield and width of the NS and AS of the azimuthal angular distribution, respectively.

1. There is no discernible double peak at the NS for any trigger or associated  $p_T$  ranges. This is possible because of the additional decay kinematics involved in producing non-prompt D-mesons from B mesons, which changes the azimuthal distribution.
2. Qualitatively, the NS peak of non-prompt  $D - \bar{D}$  correlations for all PDFs are consistent, but an AS peak for proton PDF is higher than nuclear PDFs.
3. Quantitatively, the NS yields using free proton PDFs are less than yields obtained using nPDFs

for all  $p_T^{\text{trig}}$  and  $p_T^{\text{assoc}}$  ranges, while AS yields are larger than yields obtained using nPDFs. This observation is consistent with prompt-D meson and B-meson yields. Enhancement in the NS yield suggests that gluon splitting is favored in nPDFs than in free proton PDFs while pair creation is preferred in proton PDFs compared to nuclear PDFs.

4. An interesting observation for trigger Class II and trigger Class III is observed. For  $5 < p_T^{\text{assoc}} < 10$  GeV/c yield for trigger Class II is slightly greater than trigger Class III, but for  $5 < p_T^{\text{assoc}} < 15$  GeV/c and  $5 \text{ GeV/c} < p_T^{\text{assoc}}$  range, not only Class III yield is greater than Class II, but also difference increases as we include higher  $p_T^{\text{assoc}}$  particles. This can be associated with the  $\Delta p_T$  distribution of  $b - \bar{b}$  pair created in initial hard scattering. This effect is more prominent on the AS compared to the near side, as smaller  $\Delta p_T$  is allowed on the AS due to the pair creation production process. Only nuclear PDFs demonstrated such effects for non-prompt D-mesons azimuthal correlation. The strength of this

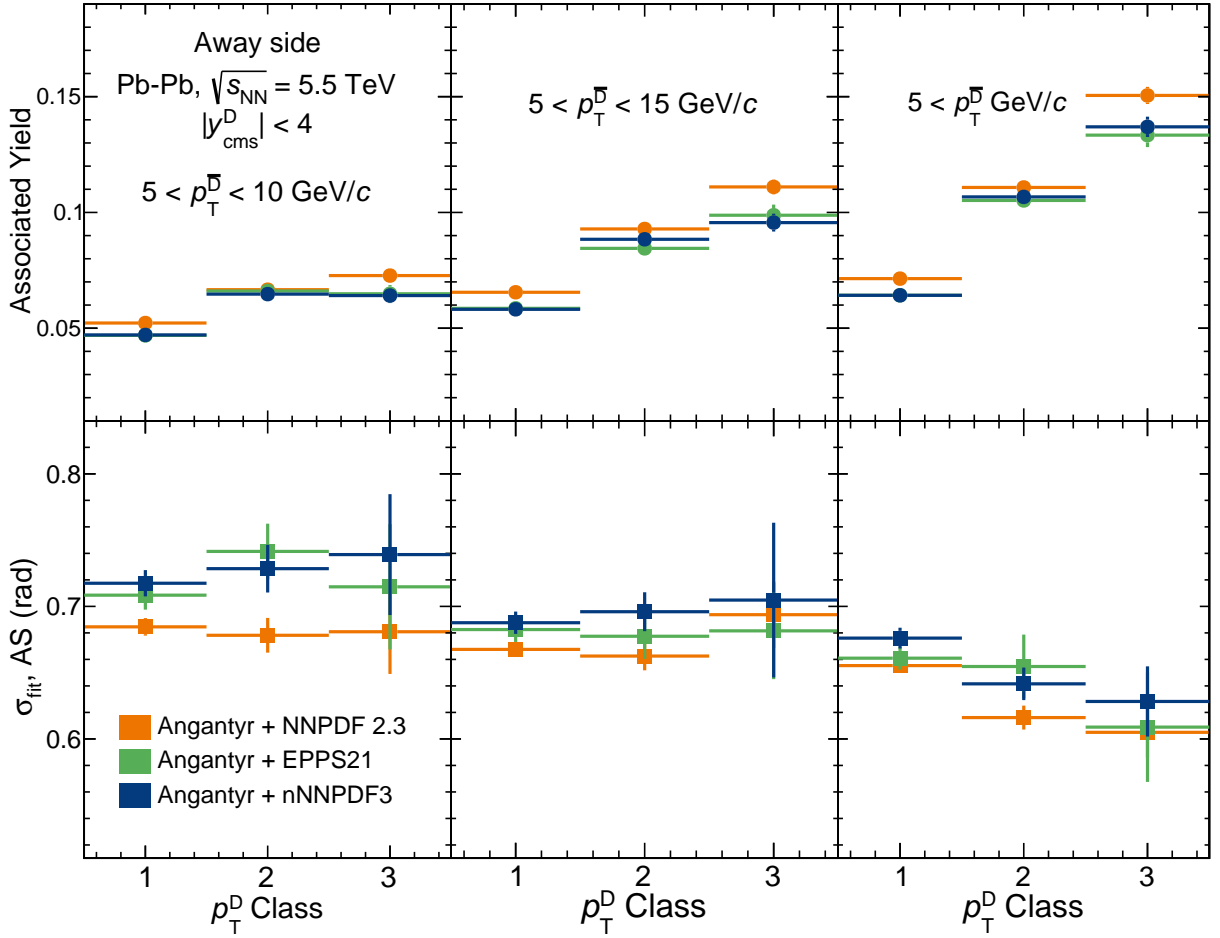


FIG. 11. Comparison of away-side yield (top row) and sigma (bottom row) for azimuthal angular correlation of non-prompt  $D - \bar{D}$  meson between free proton parton distribution function (NNPDF2.3) and nuclear PDF (EPPS21, nNNPDF3) with PYTHIA8+Angantyr in Pb-Pb collisions at  $\sqrt{s} = 5.5$  TeV.

observation is much weaker for  $D - \bar{D}$  correlation compared to  $B - \bar{B}$  correlation due to additional decay kinematics broadening the  $\Delta p_T$  distribution between a trigger and associated particles.

5. Large error bars do not allow us to make conclusive comments about PDF dependence of near-side width. In FIG 12, the NS widths show deviations of the order of 10-20% for different  $p_T^{\text{trig}}$  and  $p_T^{\text{assoc}}$  ranges, which can be associated with uncertainties of nuclear and proton PDFs.
6. For  $p_T^{\text{assoc}} > 5$  GeV/c, the width of the AS peak decreases as a function of  $p_T^{\text{trig}}$  class for all PDFs due to a higher boost. FIG 13 shows that AS widths and yields for free proton PDFs and nPDFs are consistent within uncertainties.

## V. SUMMARY

In this study, we investigate the impact of nuclear parton distribution functions (nPDFs) on the azimuthal angular correlation of  $D^0 - \bar{D}^0$ ,  $B - \bar{B}$ , and non-prompt  $D - \bar{D}$  mesons. We simulate Pb-Pb collisions at  $\sqrt{s} = 5.5$  TeV using the PYTHIA8 event generator and construct the azimuthal angular correlations of the open heavy flavor mesons by correlating the heavy quark and anti-quark pairs from the same hard scattering. By delving into this analysis, we seek to uncover potential nuclear influences on thermalization and the production of heavy quarks, both at low and high  $p_T$ . The key findings of our investigation are outlined as follows:

- Nuclear PDFs have a substantial influence on the open heavy flavor azimuthal angular correlation compared to free proton PDFs. They impact the yield and sigma of both the NS and AS of the azimuthal correlation. This occurs because nPDFs influence particle production through ISR, FSR, and MPI.

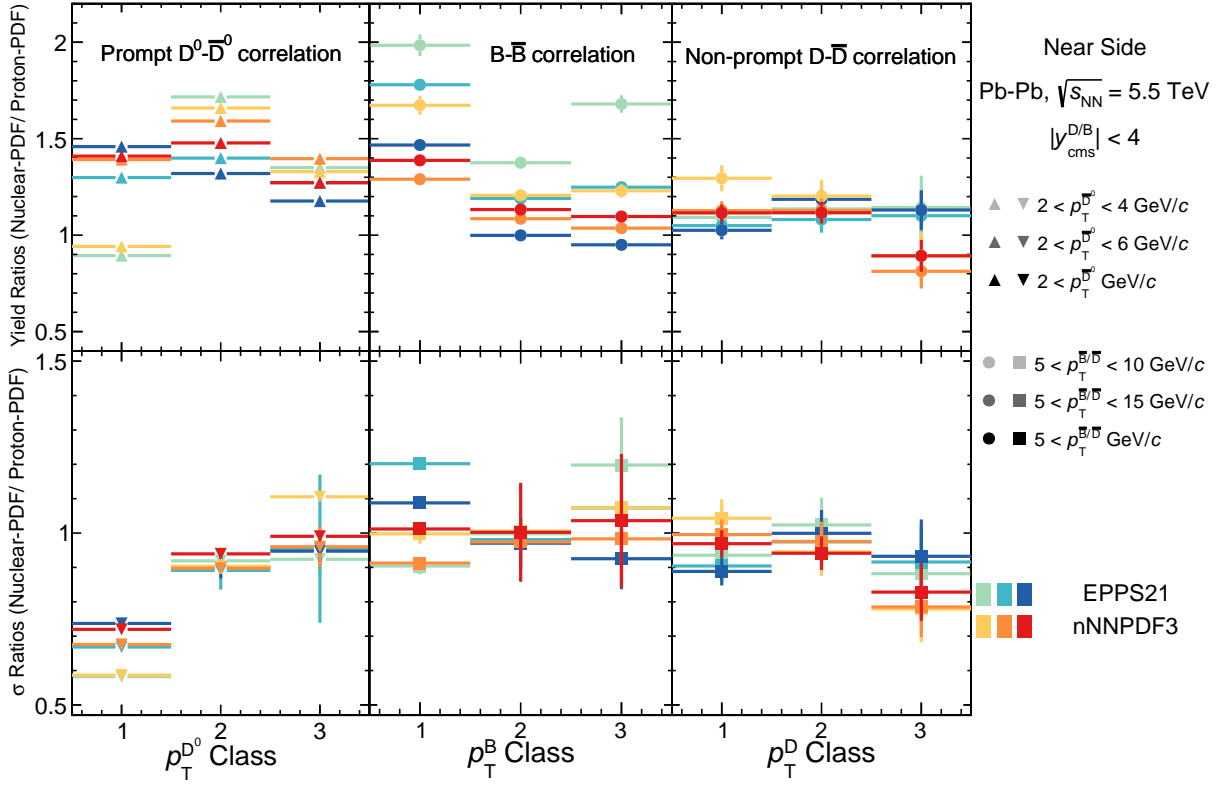


FIG. 12. Ratio of near-side yield (top row) and sigma (bottom row) of nuclear PDFs predictions to the free proton PDF predictions for  $D^0 - \bar{D}^0$ ,  $B - \bar{B}$  and non-prompt  $D - \bar{D}$  azimuthal angular correlations. The left column shows the ratios for prompt  $D^0$  meson while the middle and right columns show the ratios for B-meson and non-prompt D-mesons respectively. Numbers on the x-axis represent different  $p_T^{\text{trig}}$  classes while different shades of color represent various  $p_T^{\text{assoc}}$  ranges.

- The  $p_T$  dependent effects on the production of heavy quarks in heavy ion collisions is studied with  $p_T$  differential study of azimuthal angular correlation of open heavy flavors. It is found that the nPDFs effect depends on both  $p_T^{\text{trig}}$  and  $p_T^{\text{assoc}}$ . At low associated and trigger particle momentum, the nPDFs effects are more pronounced. A higher discrepancy at lower  $p_T$  may result from the potential sampling of the parton distribution function at low Bjorken- $x$  values, where nuclear parton distribution functions are suppressed due to the nuclear environment compared to free proton PDFs.
- One of the notable observations at the NS region was the formation of a double peak structure in the case of  $D^0 - \bar{D}^0$  and  $B - \bar{B}$  azimuthal angular correlation due to the dominant contribution from the gluon splitting process. The lack of a double peak at the near-side for non-prompt  $D^0 - \bar{D}^0$  azimuthal correlation can be attributed to decay kinematics that further change the phase space.
- Azimuthal angular correlation for  $D^0 - \bar{D}^0$ ,  $B - \bar{B}$ , and non-prompt  $D - \bar{D}$  has been found to exhibit a lower NS yield for free proton PDFs for low  $p_T^{\text{trig}}$  range than for nPDFs. This suggests that gluon splitting is more favorable for nPDFs than free proton PDFs. Compared to free proton PDFs, the AS yields for nPDFs are lower, indicating that the pair generation process is prominent in free proton PDFs.
- This work introduces a new fitting function for angular correlations. It is a convolution of Gaussian and triangular functions, suitable for different differential  $p_T$  ranges of  $B - \bar{B}$  azimuthal angular correlation. This function can handle the change in distribution shape from Gaussian-like at low  $p_T$  to triangular at high  $p_T$ .
- Using PYTHIA8, we observed non-collective effects caused by the choice of PDF in heavy-ion collisions. In the case of  $D^0$  meson, it has been observed that for  $p_T^{\text{trig}} > 4$  GeV/c and  $2 < p_T^{\text{assoc}} < 6$  GeV/c, the NS and AS sigma of azimuthal angular distribution (FIG 12, FIG 13) for both nPDFs is compatible with free proton PDF. In the lowest  $p_T^{\text{trig}}$  and  $p_T^{\text{assoc}}$  ranges, the AS distribution width increases significantly while the NS width decreases. To completely understand the thermalization of the charm quark, it is crucial to consider the impact of nPDF.
- Our investigation found no significant difference in distribution widths of  $B - \bar{B}$  azimuthal correlation

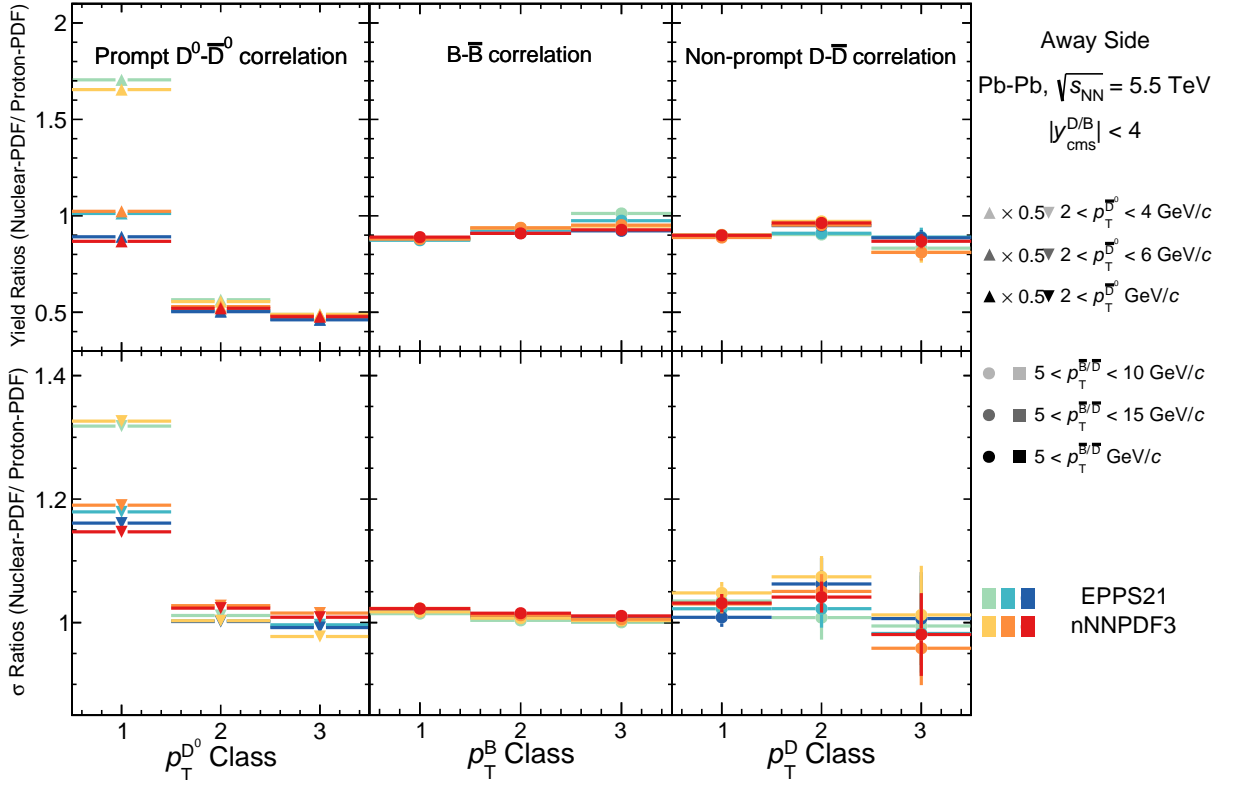


FIG. 13. Ratio of away-side yield (top row) and sigma (bottom row) of nuclear PDFs predictions to the free proton PDF predictions for  $D^0 - \bar{D}^0$ ,  $B - \bar{B}$  and non-prompt  $D - \bar{D}$  azimuthal angular correlations. The left column shows the ratios for prompt  $D^0$  meson while the middle and right columns show the ratios for B-meson and non-prompt D-mesons respectively. Numbers on the x-axis represent different  $p_T^{\text{trig}}$  classes, while different shades of color represent various  $p_T^{\text{assoc}}$  ranges.

using nPDFs compared to  $D^0 - \bar{D}^0$  azimuthal angular correlation. It could be owing to the larger mass of the beauty quark, or choices of high  $p_T^{\text{trig}}$  and  $p_T^{\text{assoc}}$  ranges, implying that nuclear PDF effects can be overlooked in the case of beauty azimuthal angular correlation studies related to thermalization and production.

Ample information about heavy flavor dynamics in small and large systems can be obtained from the detailed study of the azimuthal angular correlation of open heavy flavors. The findings of this study are observed for minimum bias Pb-Pb events, which can be extended to centrality-dependent studies with hopes for more intriguing

results and insight into additional physics.

## VI. ACKNOWLEDGEMENT

S.K. acknowledges the financial support provided by the Council of Scientific and Industrial Research (CSIR) (File No.09/1022(0084)/2019-EMR-I), New Delhi. S.K. is also grateful to the authors of PYTHIA8. R.S. acknowledges the financial support (DST/INSPIRE Fellowship/2017/IF170675) by the DST-INSPIRE program of the Government of India. The authors also thank Fabio Colamaria for fruitful discussions. This work uses computational facilities supported by the DST-FIST scheme via SERB Grant No. SR/FST/PSI-225/2016, by the Department of Science and Technology (DST), Government of India.

- [1] J. Adams *et al.* [STAR], Nucl. Phys. A **757**, 102-183 (2005) doi:10.1016/j.nuclphysa.2005.03.085 [arXiv:nucl-ex/0501009 [nucl-ex]].
- [2] P. Braun-Munzinger, V. Koch, T. Schäfer and J. Stachel, Phys. Rept. **621**, 76-126 (2016)

doi:10.1016/j.physrep.2015.12.003 [arXiv:1510.00442 [nucl-th]].

- [3] [ALICE], [arXiv:2211.04384 [nucl-ex]].
- [4] J. Adam *et al.* [ALICE], Nature Phys. **13**, 535-539 (2017) doi:10.1038/nphys4111 [arXiv:1606.07424 [nucl-ex]].

- [5] J. Barrette *et al.* [E877], Phys. Rev. Lett. **73**, 2532-2535 (1994) doi:10.1103/PhysRevLett.73.2532 [arXiv:hep-ex/9405003 [hep-ex]].
- [6] M. C. Abreu *et al.* [NA50], Phys. Lett. B **477**, 28-36 (2000) doi:10.1016/S0370-2693(00)00237-9
- [7] L. Bonino, M. Cacciari and G. Stagnitto, JHEP **06**, 040 (2024) doi:10.1007/JHEP06(2024)040 [arXiv:2312.12519 [hep-ph]].
- [8] V. G. Kartvelishvili, A. K. Likhoded and V. A. Petrov, Phys. Lett. B **78**, 615-617 (1978) doi:10.1016/0370-2693(78)90653-6
- [9] B. Andersson, G. Gustafson and B. Soderberg, Z. Phys. C **20**, 317 (1983) doi:10.1007/BF01407824
- [10] S. Acharya *et al.* [ALICE], Phys. Rev. D **105**, no.1, L011103 (2022) doi:10.1103/PhysRevD.105.L011103 [arXiv:2105.06335 [nucl-ex]].
- [11] J. Zhao, J. Aichelin, P. B. Gossiaux, A. Beraudo, S. Cao, W. Fan, M. He, V. Minissale, T. Song and I. Vitev, *et al.* Phys. Rev. C **109**, no.5, 054912 (2024) doi:10.1103/PhysRevC.109.054912 [arXiv:2311.10621 [hep-ph]].
- [12] R. J. Fries, V. Greco and P. Sorensen, Ann. Rev. Nucl. Part. Sci. **58**, 177-205 (2008) doi:10.1146/annurev.nucl.58.110707.171134 [arXiv:0807.4939 [nucl-th]].
- [13] S. Frixione, M. L. Mangano, P. Nason and G. Ridolfi, Adv. Ser. Direct. High Energy Phys. **15**, 609-706 (1998) doi:10.1142/9789812812667\_0009 [arXiv:hep-ph/9702287 [hep-ph]].
- [14] E. Norrbin and T. Sjostrand, Eur. Phys. J. C **17**, 137-161 (2000) doi:10.1007/s100520000460 [arXiv:hep-ph/0005110 [hep-ph]].
- [15] P. Braun-Munzinger, K. Redlich and J. Stachel, doi:10.1142/9789812795533\_0008 [arXiv:nucl-th/0304013 [nucl-th]].
- [16] W. M. Alberico, A. Beraudo, A. De Pace, A. Molinari, M. Monteno, M. Nardi, F. Prino and M. Sitta, Eur. Phys. J. C **73**, 2481 (2013) doi:10.1140/epjc/s10052-013-2481-z [arXiv:1305.7421 [hep-ph]].
- [17] H. Fujii and K. Watanabe, Nucl. Phys. A **920**, 78-93 (2013) doi:10.1016/j.nuclphysa.2013.10.006 [arXiv:1308.1258 [hep-ph]].
- [18] B. A. Kniehl, G. Kramer, I. Schienbein and H. Spiesberger, Phys. Rev. D **77**, 014011 (2008) doi:10.1103/PhysRevD.77.014011 [arXiv:0705.4392 [hep-ph]].
- [19] M. Salajegheh, S. M. Moosavi Nejad, H. Khanpour, B. A. Kniehl and M. Soleymaninia, Phys. Rev. D **99**, no.11, 114001 (2019) doi:10.1103/PhysRevD.99.114001 [arXiv:1904.08718 [hep-ph]].
- [20] M. Epele, C. Garcia Canal and R. Sassot, Phys. Lett. B **790**, 102-107 (2019) doi:10.1016/j.physletb.2018.11.069 [arXiv:1807.07495 [hep-ph]].
- [21] R. C. Hwa, Phys. Rev. D **22**, 1593 (1980) doi:10.1103/PhysRevD.22.1593
- [22] T. S. Biro, P. Levai and J. Zimanyi, Phys. Lett. B **347**, 6-12 (1995) doi:10.1016/0370-2693(95)00029-K
- [23] J. Ashman *et al.* [European Muon], Z. Phys. C **57**, 211-218 (1993) doi:10.1007/BF01565050
- [24] R. Aaij *et al.* [LHCb], JHEP **10**, 090 (2017) doi:10.1007/JHEP10(2017)090 [arXiv:1707.02750 [hep-ex]].
- [25] R. Aaij *et al.* [LHCb], Phys. Rev. Lett. **131**, no.10, 102301 (2023) doi:10.1103/PhysRevLett.131.102301 [arXiv:2205.03936 [nucl-ex]].
- [26] A. Kusina, J. P. Lansberg, I. Schienbein and H. S. Shao, Phys. Rev. Lett. **121**, no.5, 052004 (2018) doi:10.1103/PhysRevLett.121.052004 [arXiv:1712.07024 [hep-ph]].
- [27] [ALICE], CERN-LHCC-2020-009.
- [28] G. Aad *et al.* [ATLAS], Phys. Lett. B **802**, 135262 (2020) doi:10.1016/j.physletb.2020.135262 [arXiv:1910.13396 [nucl-ex]].
- [29] S. Acharya *et al.* [ALICE], JHEP **09**, 076 (2020) doi:10.1007/JHEP09(2020)076 [arXiv:2005.11126 [nucl-ex]].
- [30] A. M. Sirunyan *et al.* [CMS], Phys. Lett. B **782**, 474-496 (2018) doi:10.1016/j.physletb.2018.05.074 [arXiv:1708.04962 [nucl-ex]].
- [31] J. Adam *et al.* [ALICE], Phys. Lett. B **754**, 81-93 (2016) doi:10.1016/j.physletb.2015.12.067 [arXiv:1509.07491 [nucl-ex]].
- [32] S. Acharya *et al.* [ALICE], Phys. Rev. C **101**, no.4, 044907 (2020) doi:10.1103/PhysRevC.101.044907 [arXiv:1910.07678 [nucl-ex]].
- [33] J. Adam *et al.* [ALICE], JHEP **03**, 081 (2016) doi:10.1007/JHEP03(2016)081 [arXiv:1509.06888 [nucl-ex]].
- [34] S. Acharya *et al.* [ALICE], JHEP **10**, 174 (2018) doi:10.1007/JHEP10(2018)174 [arXiv:1804.09083 [nucl-ex]].
- [35] L. Adamczyk *et al.* [STAR], Phys. Rev. Lett. **113**, no.14, 142301 (2014) [erratum: Phys. Rev. Lett. **121**, no.22, 229901 (2018)] doi:10.1103/PhysRevLett.113.142301 [arXiv:1404.6185 [nucl-ex]].
- [36] S. Acharya *et al.* [ALICE], Eur. Phys. J. C **83**, no.12, 1123 (2023) doi:10.1140/epjc/s10052-023-12259-3 [arXiv:2307.14084 [nucl-ex]].
- [37] L. Adamczyk *et al.* [STAR], Phys. Rev. Lett. **118**, no.21, 212301 (2017) doi:10.1103/PhysRevLett.118.212301 [arXiv:1701.06060 [nucl-ex]].
- [38] B. B. Abelev *et al.* [ALICE], Phys. Rev. C **90**, no.3, 034904 (2014) doi:10.1103/PhysRevC.90.034904 [arXiv:1405.2001 [nucl-ex]].
- [39] B. Abelev *et al.* [ALICE], Phys. Rev. Lett. **111**, 102301 (2013) doi:10.1103/PhysRevLett.111.102301 [arXiv:1305.2707 [nucl-ex]].
- [40] S. Acharya *et al.* [ALICE], Phys. Rev. Lett. **126**, no.16, 162001 (2021) doi:10.1103/PhysRevLett.126.162001 [arXiv:2005.11130 [nucl-ex]].
- [41] A. Beraudo, A. De Pace, M. Monteno, M. Nardi and F. Prino, Eur. Phys. J. C **75**, no.3, 121 (2015) doi:10.1140/epjc/s10052-015-3336-6 [arXiv:1410.6082 [hep-ph]].
- [42] A. Adare *et al.* [PHENIX], Phys. Rev. C **99**, no.5, 054903 (2019) doi:10.1103/PhysRevC.99.054903 [arXiv:1803.01749 [hep-ex]].
- [43] L. Y. Zhang, J. H. Chen, Z. W. Lin, Y. G. Ma and S. Zhang, Phys. Rev. C **99**, no.5, 054904 (2019) doi:10.1103/PhysRevC.99.054904 [arXiv:1904.08603 [nucl-th]].
- [44] L. Y. Zhang, J. H. Chen, Z. W. Lin, Y. G. Ma and S. Zhang, Phys. Rev. C **98**, no.3, 034912 (2018) doi:10.1103/PhysRevC.98.034912 [arXiv:1808.10641 [nucl-th]].
- [45] S. Acharya *et al.* [ALICE], Eur. Phys. J. C **80**, no.10, 979 (2020) doi:10.1140/epjc/s10052-020-8118-0 [arXiv:1910.14403 [nucl-ex]].

- [46] S. Acharya *et al.* [ALICE], *Eur. Phys. J. C* **82**, no.4, 335 (2022) doi:10.1140/epjc/s10052-022-10267-3 [arXiv:2110.10043 [nucl-ex]].
- [47] J. Adam *et al.* [ALICE], *Eur. Phys. J. C* **77**, no.4, 245 (2017) doi:10.1140/epjc/s10052-017-4779-8 [arXiv:1605.06963 [nucl-ex]].
- [48] [ALICE], [arXiv:2211.02491 [physics.ins-det]].
- [49] T. Sjostrand, S. Mrenna and P. Z. Skands, *JHEP* **05**, 026 (2006) doi:10.1088/1126-6708/2006/05/026 [arXiv:hep-ph/0603175 [hep-ph]].
- [50] C. Bierlich, G. Gustafson, L. Lönnblad and H. Shah, *JHEP* **10**, 134 (2018) doi:10.1007/JHEP10(2018)134 [arXiv:1806.10820 [hep-ph]].
- [51] R. D. Ball, E. R. Nocera and J. Rojo, *Eur. Phys. J. C* **76**, no.7, 383 (2016) doi:10.1140/epjc/s10052-016-4240-4 [arXiv:1604.00024 [hep-ph]].
- [52] T. Regge, *Nuovo Cim.* **14**, 951 (1959) doi:10.1007/BF02728177
- [53] S. J. Brodsky and G. R. Farrar, *Phys. Rev. Lett.* **31**, 1153-1156 (1973) doi:10.1103/PhysRevLett.31.1153
- [54] V. N. Gribov and L. N. Lipatov, *Sov. J. Nucl. Phys.* **15**, 438-450 (1972) IPTI-381-71.
- [55] L. N. Lipatov, *Yad. Fiz.* **20**, 181-198 (1974)
- [56] G. Altarelli and G. Parisi, *Nucl. Phys. B* **126**, 298-318 (1977) doi:10.1016/0550-3213(77)90384-4
- [57] Y. L. Dokshitzer, *Sov. Phys. JETP* **46**, 641-653 (1977)
- [58] S. Barshay, C. B. Dover and J. P. Vary, *Phys. Rev. C* **11**, 360-369 (1975) doi:10.1103/PhysRevC.11.360
- [59] J. J. Ethier and E. R. Nocera, *Ann. Rev. Nucl. Part. Sci.* **70**, 43-76 (2020) doi:10.1146/annurev-nucl-011720-042725 [arXiv:2001.07722 [hep-ph]].
- [60] R. D. Ball *et al.* [NNPDF], *Eur. Phys. J. C* **77**, no.10, 663 (2017) doi:10.1140/epjc/s10052-017-5199-5 [arXiv:1706.00428 [hep-ph]].
- [61] T. J. Hou, J. Gao, T. J. Hobbs, K. Xie, S. Dulat, M. Guzzi, J. Huston, P. Nadolsky, J. Pumplin and C. Schmidt, *et al.* *Phys. Rev. D* **103**, no.1, 014013 (2021) doi:10.1103/PhysRevD.103.014013 [arXiv:1912.10053 [hep-ph]].
- [62] M. Cacciari, M. Greco and P. Nason, *JHEP* **05**, 007 (1998) doi:10.1088/1126-6708/1998/05/007 [arXiv:hep-ph/9803400 [hep-ph]].
- [63] S. Dulat, T. J. Hou, J. Gao, M. Guzzi, J. Huston, P. Nadolsky, J. Pumplin, C. Schmidt, D. Stump and C. P. Yuan, *Phys. Rev. D* **93**, no.3, 033006 (2016) doi:10.1103/PhysRevD.93.033006 [arXiv:1506.07443 [hep-ph]].
- [64] M. A. G. Aivazis, J. C. Collins, F. I. Olness and W. K. Tung, *Phys. Rev. D* **50**, 3102-3118 (1994) doi:10.1103/PhysRevD.50.3102 [arXiv:hep-ph/9312319 [hep-ph]].
- [65] K. J. Eskola, P. Paakkinen, H. Paukkunen and C. A. Salgado, *Eur. Phys. J. C* **82**, no.5, 413 (2022) doi:10.1140/epjc/s10052-022-10359-0 [arXiv:2112.12462 [hep-ph]].
- [66] R. Abdul Khalek, R. Gauld, T. Giani, E. R. Nocera, T. R. Rabemananjara and J. Rojo, *Eur. Phys. J. C* **82**, no.6, 507 (2022) doi:10.1140/epjc/s10052-022-10417-7 [arXiv:2201.12363 [hep-ph]].
- [67] R. D. Ball *et al.* [NNPDF], *Phys. Rev. D* **109**, no.9, L091501 (2024) doi:10.1103/PhysRevD.109.L091501 [arXiv:2311.00743 [hep-ph]].
- [68] R. Singh, Y. Bailung and A. Roy, *Phys. Rev. C* **105**, no.3, 035202 (2022) doi:10.1103/PhysRevC.105.035202 [arXiv:2108.08626 [nucl-th]].
- [69] T. Sjostrand, S. Mrenna and P. Z. Skands, *Comput. Phys. Commun.* **178**, 852-867 (2008) doi:10.1016/j.cpc.2008.01.036 [arXiv:0710.3820 [hep-ph]].
- [70] P. Skands, S. Carrazza and J. Rojo, *Eur. Phys. J. C* **74**, no.8, 3024 (2014) doi:10.1140/epjc/s10052-014-3024-y [arXiv:1404.5630 [hep-ph]].
- [71] J. M. Campbell, M. Diefenthaler, T. J. Hobbs, S. Höche, J. Isaacson, F. Kling, S. Mrenna, J. Reuter, S. Alioli and J. R. Andersen, *et al.* *SciPost Phys.* **16**, no.5, 130 (2024) doi:10.21468/SciPostPhys.16.5.130 [arXiv:2203.11110 [hep-ph]].
- [72] R. Corke and T. Sjostrand, *JHEP* **03**, 032 (2011) doi:10.1007/JHEP03(2011)032 [arXiv:1011.1759 [hep-ph]].
- [73] L. Lönnblad, *Nucl. Phys. A* **1005**, 121873 (2021) doi:10.1016/j.nuclphysa.2020.121873
- [74] R. Corke and T. Sjostrand, *JHEP* **01**, 035 (2010) doi:10.1007/JHEP01(2010)035 [arXiv:0911.1909 [hep-ph]].
- [75] M. Diehl, D. Ostermeier and A. Schafer, *JHEP* **03**, 089 (2012) [erratum: *JHEP* **03**, 001 (2016)] doi:10.1007/JHEP03(2012)089 [arXiv:1111.0910 [hep-ph]].
- [76] T. Sjöstrand, *Adv. Ser. Direct. High Energy Phys.* **29**, 191-225 (2018) doi:10.1142/9789813227767\_0010 [arXiv:1706.02166 [hep-ph]].
- [77] B. Andersson, G. Gustafson, G. Ingelman and T. Sjostrand, *Phys. Rept.* **97**, 31-145 (1983) doi:10.1016/0370-1573(83)90080-7
- [78] V. A. Khoze and T. Sjostrand, *Phys. Lett. B* **328**, 466-476 (1994) doi:10.1016/0370-2693(94)91506-7 [arXiv:hep-ph/9403394 [hep-ph]].
- [79] S. Gieseke, C. Rohr and A. Siodmok, *Eur. Phys. J. C* **72**, 2225 (2012) doi:10.1140/epjc/s10052-012-2225-5 [arXiv:1206.0041 [hep-ph]].
- [80] J. Rathman, *Phys. Lett. B* **452**, 364-371 (1999) doi:10.1016/S0370-2693(99)00291-9 [arXiv:hep-ph/9812423 [hep-ph]].
- [81] C. Bierlich and J. R. Christiansen, *Phys. Rev. D* **92**, no.9, 094010 (2015) doi:10.1103/PhysRevD.92.094010 [arXiv:1507.02091 [hep-ph]].
- [82] J. R. Christiansen and P. Z. Skands, *JHEP* **08**, 003 (2015) doi:10.1007/JHEP08(2015)003 [arXiv:1505.01681 [hep-ph]].
- [83] C. Bierlich, G. Gustafson and L. Lönnblad, *JHEP* **10**, 139 (2016) doi:10.1007/JHEP10(2016)139 [arXiv:1607.04434 [hep-ph]].